# Protonated N-Confused Porphyrin Dimer: Formation, Structure, and Guest Binding[†]

Piotr J. Chmielewski,* Marta Siczek, and Ludmiła Szterenberg

Department of Chemistry, University of Wrocław, F. Joliot-Curie 14, 50 383 Wrocław, Poland

S Supporting Information

ABSTRACT: The protonation of 3,3′-bis(*meso*-tetratolyl-2-aza-21-carbaporphyrin) with various acids was studied. The stepwise formation of mono-, di-, and tetracationic species was shown on the basis of UV−vis−near-IR and low-temperature ^{1}H NMR. Upon going from di- to tetraprotonated form, the bis(porphyrinoid) skeleton changes its conformation from cisoid to bent-transoid, which was found by single-crystal X-ray analyses, 2D NMR, and density functional theory (DFT) calculations. The formation of cation−anion complexes was established in both the solid state and solution. The substitution of anions was studied by spectrophotometric and ^{1}H NMR titrations. A pronounced decrease of the HOMO−LUMO gap in the tetraprotonated species was shown by cyclovoltametry and time-dependent DFT calculations.
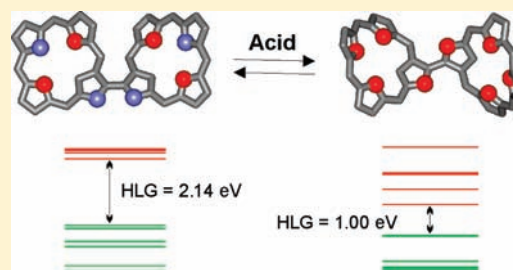
INTRODUCTION

For many potential ligands, particularly for nitrogenous bases, protonation can be used in the process of searching for accessible donor sites and in the determination of their number, position, and basicity. Protonation appears to be a simple addition reaction, although the results of attaching hydrogen cation(s) can severely influence the structure of the base mostly by perturbing the electron density distribution within the acceptor molecule, usually in a reversible manner. The accompanying anion neutralizes the positive charge, but it also participates in an acid−base equilibrium competing with the protonation object and can interact with a charged protonated system by attractive electrostatic forces and hydrogen bonds. Such noncovalent interactions between guest molecules or ions and compatible hosts are of primary importance for the formation of supramolecular adducts and have been widely studied in last 4 decades, aiming at the preparation of effective and selective receptors and sensors. Among countless systems forming complexes with anions,[1−18] there are porphyrins and porphyrin analogues and homologues[16] that belong to a subclass of macrocycles interacting with anions in the protonated states.[19] Although many reports concerning anion binding are available for the so-called "expanded porphyrins", particularly for oligopyrroles consisting of five or more pyrrole subunits,[16,20−24] there is a relatively low number of protonated tetrapyrrolic systems for which stable complexes with anions are formed, and they can be characterized in the solid state rather than in solution.[25−29] Protonation of porphyrins is combined with distortion of the planar structure of aromatic tetrapyrroles, which is not suitable for the adaptation of four hydrogen atoms inside the crevice because of spatial overcrowding. Thus, the apparent basicity of the porphyrin core is lowered unless tilting of the pyrrole subunits out of the common plane is a preexisting feature of the macrocyclic ring, which is usually caused by substituents located on the perimeter.[28,30] In the case of the porphyrin isomer, N-confused porphyrin (NCP) **1**, there are three hydrogen atoms already in the neutral form, resulting in a nonplanar structure of this tetrapyrrole in the solid state,[31] which may suggest a higher effective basicity of this macrocycle. However, the presence of a basic site on the perimeter in the structure of **1** (Chart 1) appreciably changes the protonation pattern of this macrocycle with respect to regular tetrapyrroles. With a few exceptions of monoacid formation,[32] the protonation of porphyrins proceeds in a concerted manner; i.e., both basic sites are protonated simultaneously. In the case of NCP, the process involves two or three well-separated steps,[33,34] where the external nitrogen atom of the *confused* pyrrole (N2) is a primary target of protonation owing to its exposed position and lack of further significant distortion combined with the attachment of a proton. In fact, a unique property of the neutral form of NCP is the formation of a tautomer with a proton attached to N2, which is stabilized by hydrogen bonds with dipoles or anions.[35−37]

Properties such as the electronic structure, flexibility, and adaptability of the systems consisting of two directly linked porphyrin subunits[38−46] depend on several factors, among which the mobility of the bipyrrole moiety seems to be of primary importance in the case of β-β'-linked bis(porphyrins).[47−49] The factors determining the stability of the molecule's configuration are important because of the intrinsic chirality of these bis-(porphyrins). The structural and some of the coordination properties of 3,3′-bis(*meso*-tetraaryl-2-aza-21-carbaporphyrin) (**2**) remain analogous to those of a regular β-β'-linked bis-(porphyrin), with the obvious differences related to the presence of nitrogen on the perimeter of each of the subunits in the vicinity

Chart 1

Ar = *p*-Tol
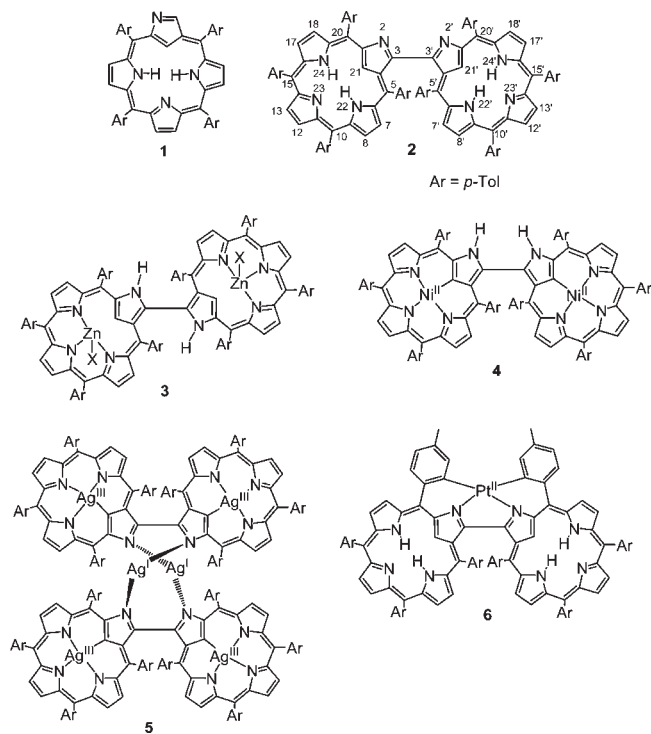
of the bridging bond. The structure of **2** consists of two NCP subunits that are almost coplanar, and nitrogen atoms of the *confused* pyrroles are in the cisoid conformation.[50] A steric hindrance introduced by the neighboring aryls prevents free rotation around the bond linking the subunits. Thus, the transition from the cisoid to transoid arrangement requires a simultaneous movement of both *confused* pyrroles with respect to the macrocyclic rings. Such structural change has been observed upon metalation of **2** with zinc, yielding **3**,[51] while for nickel(II) and silver(III) complexes **4** and **5**, the cisoid conformation is preserved by coordination of the inner carbon atoms of the *confused* pyrroles.[52] Another way of preventing rotation is coordination to the system of external nitrogen atoms of the moiety that has been shown for platinum(II) complex **6**, where macrocyclic crevices of both subunits are unoccupied and the metal ion is doubly orthometalated by aryls adjacent to the chelating bipyrrole.[53]

In this paper, we present studies on the behavior of **2** upon protonation that appears to be not merely a hydrogen cation addition to the four basic sites of bis(NCP) but a process connected with appreciable structural and spectroscopic alteration as well as with binding of anionic and neutral guests in the solid state and in solution.

■ RESULTS AND DISCUSSION

Protonation of (NCP)₂. An Overview. Bis(NCP) comprises four basic sites that can be protonated: two external nitrogen atoms of the bipyrrole fragment and two nitrogen atoms inside the macrocyclic subunits. One can expect that the gradual addition of an acid to the solution of **2** will follow to some extent a protonation pattern of monomeric NCP.[33] However, the proximity of the basic sites and possible interaction between the macrocyclic subunits likely introduces important distinctions

between the behaviors of isolated NCP and bis(NCP) upon protonation. There are thus several points that should be taken into account during analysis of the acidification of **2**. (1) Either the respective sites of the subunits can accept protons independently or introduction of the proton into one part can influence the protonation of the other part. (2) The structure of the bis(porphyrin) may change upon protonation by alteration of the relative orientation of the subunits. (3) Anionic and/or polar neutral species complexation is likely for the highly charged tetracationic species. The systematic titrations of **2** with acids monitored by ¹H NMR spectroscopy allow identification of the consecutively formed cations if the chemical exchange between them is slow on the NMR time scale. Thus, experiments were carried out at low temperature, i.e., 213 K for CDCl₃ and 173 K for CD₂Cl₂ solutions of **2**. Trifluoroacetic acid (TFAH) and hydrogen chloride (dry HCl in a CDCl₃ solution) were chosen for the systematic study of the gradual protonation of bis(NCP).

Figure 1 presents selected spectra taken upon the addition of TFAH. Apart from the neutral form (n), there are three protonated species that can be identified in the solution (Scheme 1): monocation (m)⁺, dication (d)²⁺, and tetracation (q)⁴⁺. The monocation (m)⁺ is characterized by the lack of 2-fold symmetry, which is present in the neutral form. The proton is localized on the external nitrogen atom of one of the subunits, which gives rise to a signal of 2-NH, which appears in the low-field at about 18 ppm. In the high-field region of the spectrum, there are two signals of 21-CH and four signals of the internal NH protons. The integral intensities of all of these resonances are equal. The signals were assigned on the basis of 2D correlation experiments (COSY and NOESY) performed for a carefully overcooled CD₂Cl₂ solution of monocation at 173 K, where NH resonances are sharper owing to slower chemical exchange. The asymmetry of the monoprotonated species indicates that only one of the nitrogen atoms of the bipyrrolic system is involved in the proton bonding at this stage and that the dynamic effects do not average its position at low temperature. Such chemical exchange effects are observed for the titration carried out at 253 K, where only one set of signals of monocation (m)⁺ is observed. In fact, chemical exchange is also documented at low temperatures by correlation signals observed in the NOESY spectrum for the respective protons belonging to different subunits of the monocation, e.g., for two 21-CH, two 22-NH, or one 5Me (Figure S1 in the Supporting Information).

Although the monocation (m)⁺ cannot be observed as a unique species in solution and it is always accompanied by the preceding neutral form (n) and/or proceeding dication (d)²⁺, a concentration range of its occurrence and domination is rather broad, allowing observation of (m)⁺ even after the addition of 3 equiv of acid at 213 K. This may reflect an interaction between the closely spaced protonation sites on the bipyrrolic moiety as the second proton is localized in (d)²⁺ on the external nitrogen of the other subunit. Such localization can be inferred from the 2-fold symmetry of the dication, which is represented by only one set of signals in all regions of the spectrum. Also, the dication can be observed only as a component of a mixture along with the lower and higher protonated species.

Further protonation takes place inside the macrocyclic crevices. Only one set of new signals appears upon an increase in the acid concentration. Chemical shifts of the signals assigned to the consecutive protonated form do not vary until the equilibrium saturation point is reached, which proves that chemical exchange is slow on the NMR time scale. This clearly indicates the
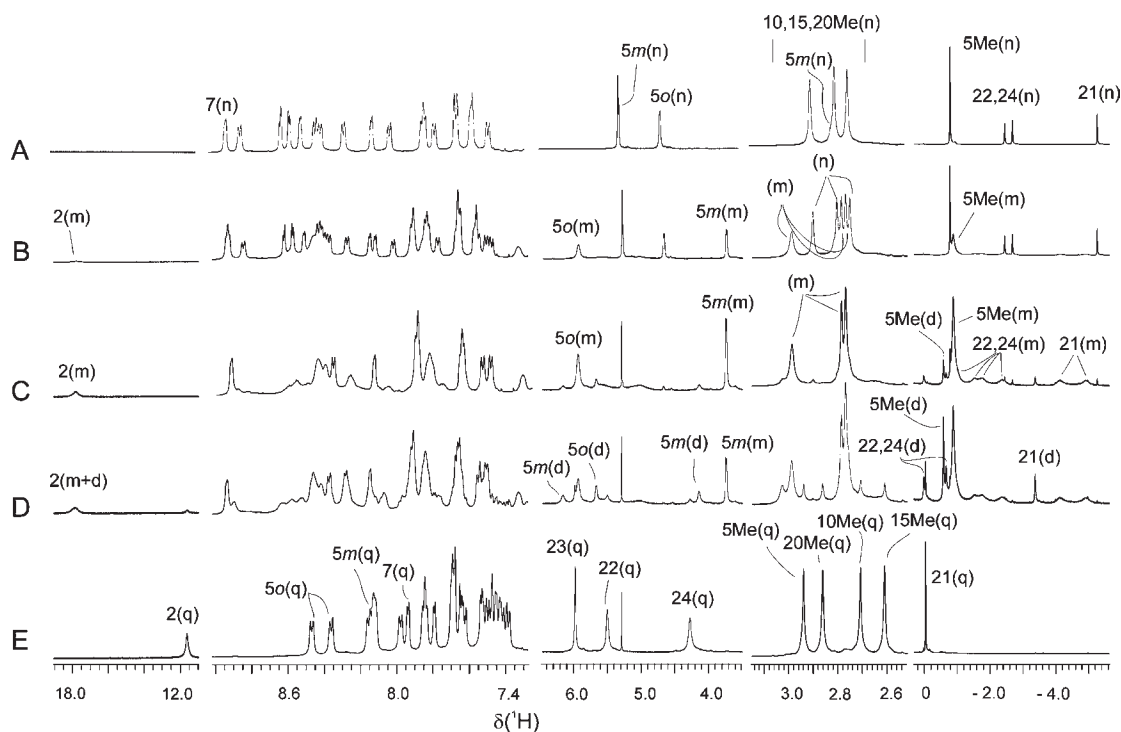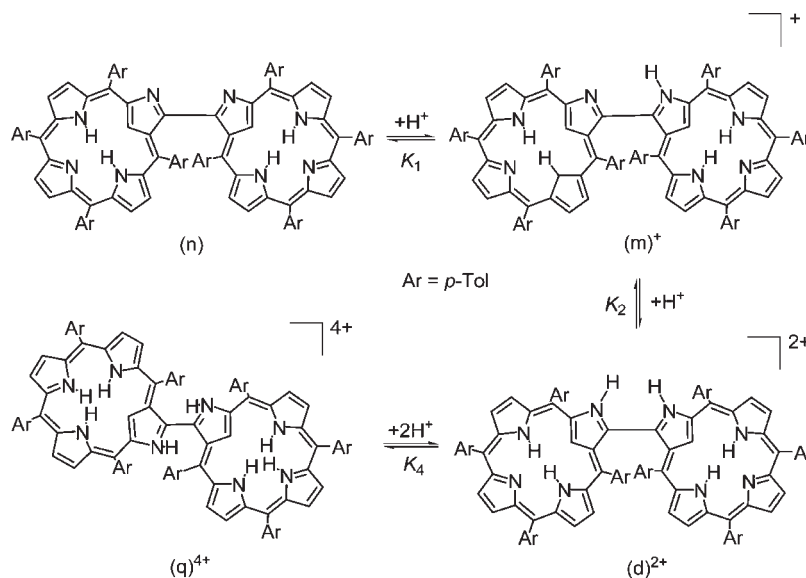
Figure 1. Selected ^1H NMR spectra (500 MHz, 213 K, CDCl$_3$) taken upon titration of **2** with TFAH: (A) no acid added; (B) 0.5 equiv; (C) 1 equiv; (D) 2 equiv; (E) 5 equiv. The signal assignments follow that of Chart 1 for (n) neutral **2**, (m) monocation, (d) dication, and (q) tetracation.

Scheme 1. Protonation Equilibria for Bis(NCP)

formation of symmetric tetracation $(q)^{4+}$ without a preceding trication. Thus, protonations of the interiors of both subunits occur simultaneously, which can be accounted for by the equivalent character of two internal basic sites and by a lack of electrostatic interaction between them.

The similar protonation pattern is observed upon the addition of a HCl solution in CDCl$_3$; however, significant differences occur regarding the molar ratios of differently protonated forms. Unlike in the case of TFAH for which the molar contribution of the

2,2′-protonated dication reaches 35% upon the addition of about 1.5 equiv of the acid, a maximum mole ratio of this symmetric form is less than 4% when hydrogen chloride is used as a source of protons. In the Figure 2, speciations of the protonated forms observed upon titration of **2** with TFAH or HCl by means of ^1H NMR (CDCl$_3$, 213 K) are presented, indicating only a minute amount of dication $(d)^{2+}$ in the whole range of the HCl concentration.

The observed differences in the relative stabilities of cationic forms between systems with TFAH and HCl can indicate the
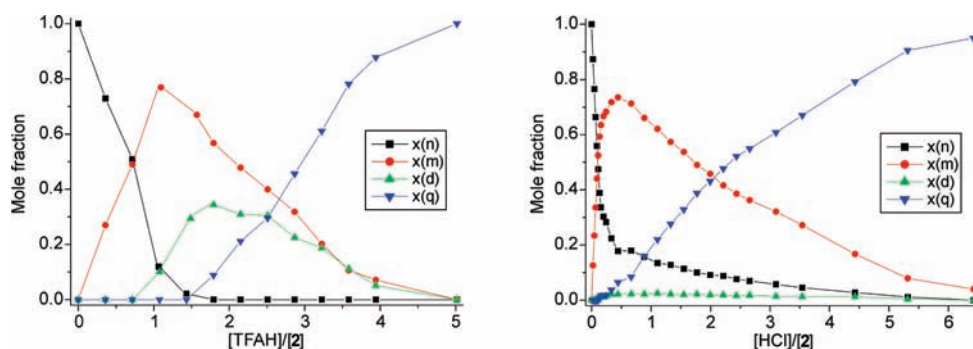
Figure 2. Distribution of the forms observed upon titration of **2** with TFAH (left) or HCl (right). The speciations were determined by means of integral intensities of the ^{1}H NMR signals in the spectra taken at different acid concentrations (CDCl$_3$, 213 K). Assignments: n, neutral form; m, monocation; d, dication; q, tetracation.

interaction of protonated species with anions. Such interaction is reflected by different spectral parameters, which are most pronounced for tetracation (see below) but can be observed also for chemical shifts of some of the protons in mono- and dications at low temperature (see Table S1 in the Supporting Information).

Some of the differences between the systems can be related to the various strengths of the acids. Only the tetracationic form is observed by ^{1}H NMR spectroscopy for the samples acidified with HCl in the temperature range of 213−300 K under the conditions of saturation of the equilibrium K_4, while for the solution containing **2** and 5 equiv of TFAH, an increasing dication concentration is observed when the temperature is raised above 273 K. This reflects a difference in the basicity of TFA$^-$ and Cl$^-$. The competition between anion and "internal" nitrogen atoms is even more evident for dichloroacetic acid (DCAH) used as a proton source. Variable-temperature ^{1}H NMR experiments for the solution consisting of **2** and 4 equiv of DCAH indicate partial deprotonation of (q)$^{4+}$ above 233 K, resulting in the presence of diprotonated species (d)$^{2+}$. The relative 21-H signal intensities of tetra- and diprotonated complexes allow estimation of their molar ratios in the temperature range of 233−283 K owing to a slow chemical exchange between these species. Above 283 K, only the dication complex is observed. The values of the thermodynamic functions for the equilibrium K_4, as obtained by means of the van't Hoff equation, are estimated as $\Delta H^\circ = -21.1\ (\pm 0.4)$ kcal/mol and $\Delta S^\circ = -51\ (\pm 2)$ cal/(mol·K) (see Figure S2 in the Supporting Information for details).

Spectrophotometric titrations of **2** in a chloroform solution (Figure 3) allow estimation of the equilibrium constants for the systems with TFAH and DCAH (Table 1), and variable-temperature experiments in the range of 280−333 K, followed by van't Hoff dependence analyses, bring information concerning thermodynamic functions ΔH° and ΔS° for these equilibria (Table 1). Significant differences between the equilibrium constants for the systems with TFAH and DCAH reflect the different acidities of these carboxylic acids (pK_a = 0.23 for TFAH[54] and 1.25 for DCAH[55]). As expected, attachment of the first proton to bis(NCP) is more effective than attachment of the second ($K_1 > K_2$), and a cumulative constant, K_1K_2, for the two initial protonation steps is significantly greater than K_4. On the other hand, both K_1 and K_2 vary only slightly with temperature, which results in moderately negative standard enthalpy changes for the processes of mono- and dication formation and in small, but positive, standard entropy changes for both acids (Table 1). The temperature dependence of K_4 is appreciably more pronounced.

The much more negative values of the thermodynamic functions observed for binding of the second pair of protons suggest that an exothermic, but remarkably antientropic process accompanies protonation of the internal basic sites of bis(NCP). This likely reflects the formation of an ordered structure of a cation−anion complex, which is more effective for a tetracationic species than for mono- or dication.

There are no further alterations in the ^{1}H NMR spectra at 213 K when the concentration of HCl is considerably exceeding the stoichiometric ratio required for the tetracation, while in the case of titration of **2** with TFAH, a broadening of all signals of the fully protonated bis(NCP) is observed already upon the addition of 5.5 equiv of the acid. This suggests an equilibrium involving the tetracation and un-ionized molecules of TFAH. A similar effect is observed for DCAH as a proton source at 213 K. Spectral changes occurring upon spectrophotometric titration with both TFAH and DCAH at 298 K in a concentration range exceeding 100 equiv of the acid can also suggest such an interaction.

The low-temperature ^{1}H NMR-monitored titration of **2** with HCl reveals interaction of the cationic forms with water present in the solvent. For the CDCl$_3$ solutions, a resonance of dissolved water appears in the region of δ 1.5−1.8 depending on the temperature, and a lowering of the temperature causes a downfield shift of its signal. At 213 K, water resonates at δ 1.78 in the chloroform solution of **2** and its position is gradually shifted to higher frequencies upon the addition of a HCl solution up to δ 2.6 (Figure S3 in the Supporting Information), and then the signal is shifted back to the final value of about δ 1.2. A decrease from the maximum value of the chemical shift starts from the acid concentration for which signals of the tetracationic form appears for the first time in the titration. This strongly suggests that water molecules are associated with (q)$^{4+}$. This interaction can be interpreted as hydrogen bonding between protonated nitrogen atoms as donors and an oxygen atom as an acceptor. The shielding influence of the aromatic rings is responsible for the observed upfield shift. The presence of only one signal of water indicates fast exchange between "free" water and that associated with (q)$^{4+}$. A similar effect is observed upon titration of **2** with TFAH, although variation of the water signal position in this case is much smaller (1.79−1.89 ppm). Also, low-temperature NOESY experiments performed for tetracations reveal an association of water molecules with the quadruply protonated dimer. Strong correlations of the water signal with ortho protons of the *meso*-aryl substituents in positions 5 and 20 as well as with the β-pyrrole proton in position 7 indicate a specific interaction of the
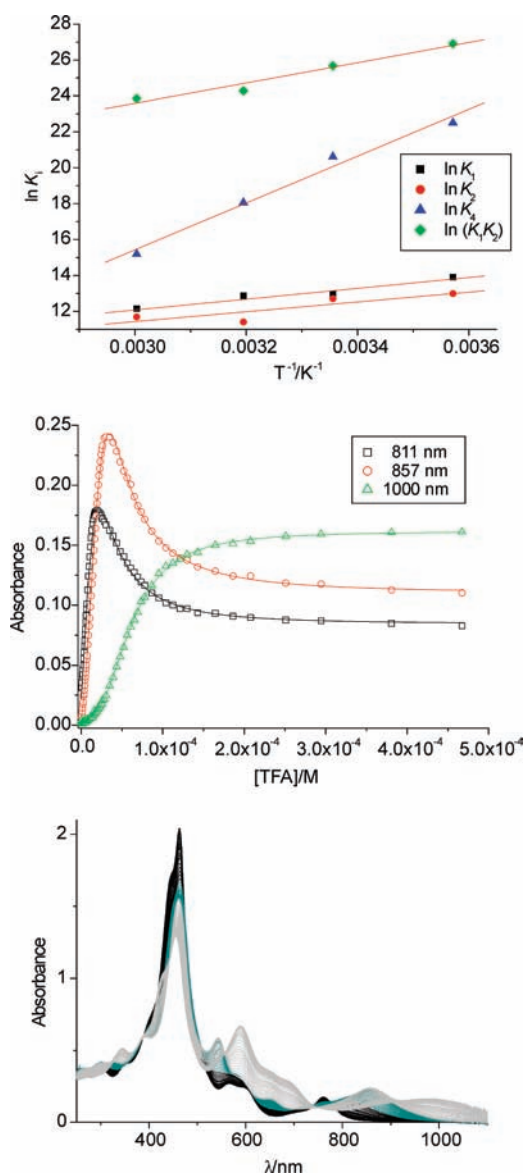
Figure 3. Bottom: Optical spectra of **2** ($c_0 = 1.27 \times 10^{-5}$ M, CHCl$_3$, 298 K) recorded upon titration with TFAH. Black traces are those recorded for the solutions containing mainly (n) and (m)$^+$, cyan traces represent spectra of (m)$^+$ and (d)$^{2+}$ equilibrium mixtures, and light gray traces represent those of (d)$^{2+}$ and (q)$^{4+}$. Middle: Absorbance dependencies at three specified wavelengths reflecting changes in the concentrations of various protonated forms upon titration of **2** with TFAH at 298 K. Solid lines are calculated by means of a nonlinear curve fitting to the experimental points. Top: van't Hoff plots for the specified protonation equilibrium constants derived from titrations of **2** with TFAH in the temperature range of 280–333 K.

tetracation with water molecules and its location close to the external nitrogen atom of the *confused* pyrrole (Figure S4 in the Supporting Information).

In summary to this overview, we show that protonation of **2** proceeds through three steps of mono-, di-, and tetracation in which external and internal nitrogen atoms are involved. Interactions of the protonated species with anions result in differentiation of the relative stability of the forms and in different spectral properties. The hydration of tetracation can be observed for its adduct with chloride (q)Cl$_4$, while interaction with

un-ionized molecules of acid is also likely in the case of TFAH and DCAH.

Structures in the Solid State. Single-crystal X-ray analyses for **2** and its protonation products reveal different arrangements of the subunits in the free base or dication and in the tetracation (Tables 2, 3, and 5 and Figure 4). While structural features observed for **2** or **2**(HCl)$_2$ indicate a cisoid conformation in the crystal, in the quadruply protonated **2**(HCl)$_4$(H$_2$O)$_2$, the bis-(porphyrinoid) adopts a bent transoid conformation (Tables 4 and 5). Although the molecules are intrinsically chiral, they crystallize in the centrosymmetric space groups and thus form racemic phases. The average distances between nitrogen and carbon atoms in the respective structural fragments of **2** and its protonated homologues do not differ beyond 3σ except for the N2–C3 bond, which is about 0.03 Å shorter in the free base (Table 2). On the other hand, the C–N–C bond angles in the pyrrole rings with hydrogen-bearing nitrogen atoms are about 4° higher than in those without hydrogen attached to nitrogen. Thus, this angle in the *confused* pyrrole, i.e., C1–N2–C3, increases upon the addition of a proton to N2 upon going from **2** to **2**(HCl)$_2$, while protonation of N23 causes a higher value of the C11–N23–C14 angle in the tetracation **2**(HCl)$_4$(H$_2$O)$_2$ than those observed for its predecessors (Table 2). In all three structures, there are small molecules and/or anions for which a hydrogen-bonding interaction with the dimer can be ascertained based on the close interatomic distances and proper angles (Table 3). Even in the case of the free base, there is a molecule of methanol that donates hydrogen to the external nitrogen of one of the subunits (N2), while the other external nitrogen (N26) seems to interact with a chloroform molecule, which results in asymmetry of the whole molecular system. In contrast to the free base of **2**, the solid-state structure of its diprotonated form **2**(HCl)$_2$ possesses 2-fold symmetry. The chloride anion Cl1 of the asymmetric part of the structure is solvated by two chloroform molecules and localized in the distance of 3.002(6) Å from the external nitrogen N2, which indicates a hydrogen-bonding interaction. Crystallization of this adduct is somewhat surprising considering its low relative stability and thus minute molar fraction in solution at low temperature (Figure 2). The symmetry of **2**(HCl)$_4$(H$_2$O)$_2$ is also 2-fold, although two chloride anions that can be found in the asymmetric part are not equivalent. The anions are localized on the opposite inequivalent faces of each subunit. One chloride resides outside the cleft formed by the subunits interacting with N23, with shortest H···A and D···A distances among the Cl–N hydrogen bonds formed in this system. The Cl1–C21 distance [3.498(6) Å] seems to be too long for the C–H···Cl hydrogen bond. The other chloride participates in an array of hydrogen bonds, interacting with two "internal" nitrogen atoms (N22 and N24) and with a water molecule. This molecule is also an acceptor in the hydrogen bond with the "external" nitrogen (N2) of the other subunit of the dimer. The structure of the bis(porphyrin) fragment resembles an open shell of a bivalve; however, unlike in the case of the mollusks, which consist of heterochiral subunits and are thus achiral, the molecule of **2**(HCl)$_4$ is constituted of homochiral "halves".

For all three molecules, there is a saddle-shaped distortion of the macrocyclic subunits, with the pairs of perimeter pyrrole atoms located alternatively above and beyond a mean plane P$_{21}$ defined by 21 heavy atoms (i.e., all ring atoms except N2, C3, and C21). The mean atom displacement from this plane is 0.21 Å in **2**, 0.28 Å in **2**(HCl)$_2$, and 0.37 Å in **2**(HCl)$_4$(H$_2$O)$_2$. The most

Table 1. Equilibrium Constants and Values of the Thermodynamic Functions for the Reaction of 2 with TFAH and DCAH in Chloroform

T [K]	K_1 ($\pm$sd) [M^{-1}]	K_2 ($\pm$sd) [M^{-1}]	K_4 ($\pm$sd) [M^{-2}]	K_1K_2 [M^{-2}]
		TFAH		
280	1.1 ($\pm$0.2) $\times$ 10^6	4.4 ($\pm$1.2) $\times$ 10^5	6.2 ($\pm$0.2) $\times$ 10^9	4.8 $\times$ 10^{11}
298	4.3 ($\pm$0.2) $\times$ 10^5	3.3 ($\pm$0.6) $\times$ 10^5	9.0 ($\pm$0.5) $\times$ 10^8	1.4 $\times$ 10^{11}
313	3.9 ($\pm$0.3) $\times$ 10^5	9.0 ($\pm$1.1) $\times$ 10^4	7.1 ($\pm$0.3) $\times$ 10^7	3.5 $\times$ 10^{10}
333	1.9 ($\pm$0.1) $\times$ 10^5	1.1 ($\pm$0.2) $\times$ 10^5	3.9 ($\pm$0.3) $\times$ 10^6	2.1 $\times$ 10^{10}
$\Delta H°$ ($\pm$sd) [kcal/mol]	-6 (1)	-5.4 (2.0)	-26 (2)	-11.3 (1.6)
$\Delta S°$ ($\pm$sd) [cal/(mol·K)]	6 (3)	6 (6)	-48 (8)	13.4 (5.4)
		DCAH		
283	2.2 ($\pm$0.2) $\times$ 10^5	2.0 ($\pm$0.5) $\times$ 10^4	1.0 ($\pm$0.1) $\times$ 10^7	4.4 $\times$ 10^9
298	1.6 ($\pm$0.3) $\times$ 10^5	1.4 ($\pm$0.2) $\times$ 10^4	1.4 ($\pm$0.2) $\times$ 10^6	2.2 $\times$ 10^9
313	7.3 ($\pm$0.2) $\times$ 10^4	1.1 ($\pm$0.2) $\times$ 10^4	1.0 ($\pm$0.2) $\times$ 10^6	8.0 $\times$ 10^8
$\Delta H°$ ($\pm$sd) [kcal/mol]	-6.4 (1.7)	-3.5 (0.3)	-27 (3)	-10.0 (1.5)
$\Delta S°$ ($\pm$sd) [cal/(mol·K)]	2 (6)	7 (1)	-63 (10)	9 (5)

Table 2. Selected Bond Distances and Angles from Single-Crystal X-ray Structures of 2, 2(HCl)$_2$, and 2(HCl)$_4$(H$_2$O)$_2$

atoms	2	2(HCl)$_2$	2(HCl)$_4$(H$_2$O)$_2$
	Bond Distances [Å]		
C1−N2	1.416(3), 1.411(3)^a	1.385(9)	1.398(6)
N2−C3	1.313(3), 1.314(3)^a	1.348(9)	1.348(6)
C6−N22	1.387(3), 1.387(3)^a	1.39(1)	1.385(7)
N22−C9	1.371(3), 1.361(3)^a	1.35(1)	1.357(7)
C11−N23	1.375(3), 1.371(3)^a	1.34(1)	1.373(7)
N23−C14	1.384(3), 1.378(3)^a	1.38(1)	1.371(7)
C16−N24	1.364(3), 1.369(3)^a	1.37(1)	1.360(7)
N24−C19	1.385(3), 1.376(3)^a	1.38(1)	1.372(7)
C1−C21	1.407(3), 1.401(3)^a	1.36(1)	1.383(7)
C21−C4	1.403(3), 1.398(3)^a	1.43(1)	1.401(7)
C3−C3$'$	1.476(3)	1.46(1)	1.44(1)
	Bond Angles [deg]		
C1−N2−C3	106.2(2), 105.5(2)^a	109.1(6)	109.9(4)
C6−N22−C9	111.0(2), 111.4(2)^a	111.6(7)	110.0(4)
C11−N23−C14	105.4(2), 104.9(2)^a	104.5(7)	109.6(4)
C16−N24−C19	110.8(2), 111.0(2)^a	110.4(6)	110.5(4)
C1−C21−C4	107.8(2), 107.5(2)^a	108.4(6)	109.2(4)

^{a} Parameter for atoms with numbering shifted by 24 with respect to that in the first column of the table.

Table 3. Hydrogen Bond Geometries in the Crystal Structures of 2, 2(HCl)$_2$, and 2(HCl)$_4$(H$_2$O)$_2$

D−H···A	D−H [Å]	H···A [Å]	D···A [Å]	D—H···A [deg]
		2		
O1R−H1R···N2	0.84	2.09	2.878(3)	156
C1A−H1A···N26	1.00	2.20	3.185(3)	170
		2(HCl)$_2$		
C1A−H1A···Cl1	1.00	2.48	3.438(9)	160
C1B−H1B···Cl1	1.00	2.23	3.22(1)	172
N2−H2···Cl1	0.88	2.31	3.002(6)	136
		2(HCl)$_4$(H$_2$O)$_2$		
N2−H2···O1W	0.88	1.91	2.739(6)	156
N22−H22···Cl2	0.88	2.45	3.252(5)	151
N23−H23A···Cl1	0.88	2.35	3.091(5)	143
N24−H24···Cl2	0.88	2.44	3.180(5)	141
O1W−H1W···Cl2^a	0.86	2.25	3.075(4)	160

^{a} Symmetry code: $-x + 1$, y, $-z + \frac{1}{2}$.

significant saddle-shaped distortion of subunits is observed in 2(HCl)$_4$(H$_2$O)$_2$, which is caused by the presence of four protons inside the macrocycle crevices (Figure 5). Such a distortion is similar to that observed for the bis(chloride) complex of regular porphyrin.[26]

Structures in the Gas Phase and in Solution. The observation of different orientations of the subunits in the solid state for 2 and 2(HCl)$_4$ implies a possibility of rearrangement of the molecule's shape in solution. The ^{1}H NMR spectroscopy appeared to be sensitive to such an alteration of the structure owing to the aromatic character of the macrocyclic fragments of the system and can be very useful, in particular, when correlated with theoretical predictions. A molecular modeling on the B3LYP6-31G** level of differently protonated forms of 2 was used for

estimation of the relative energies of various conformers, and the results were confronted with the experimental solid-state and solution data. Orientation of the subunits with respect to each other is defined by a conformation of the bipyrrole moiety reflected by the N2−C3−C3$'$−N2$'$ torsion angle (TA$_{NCCN}$), a dihedral angle between the mean planes of the *confused* pyrroles (DA$_{CC}$), and a dihedral angle DA$_{2121}$ between the mean planes P$_{21}$ defined by 21 atoms including those of *regular* pyrroles, meso bridges, and carbon atoms C1 and C4 in each subunit. An interconversion of the structures, e.g., enantiomerization, formally involves rotation around a single bond of bipyrrole and alteration of a dihedral angle DA$_{21C}$ between the plane of *confused* pyrrole and the mean plane P$_{21}$ in both subunits. A restriction in the rotational freedom around the unique bond C3−C3$'$ caused by the proximity of *meso*-aryls in positions 5 and 20 of both subunits results in three feasible types of structures that constitute local minima separated by rotational barriers in the conformational space (Table 4). In an axially chiral cisoid
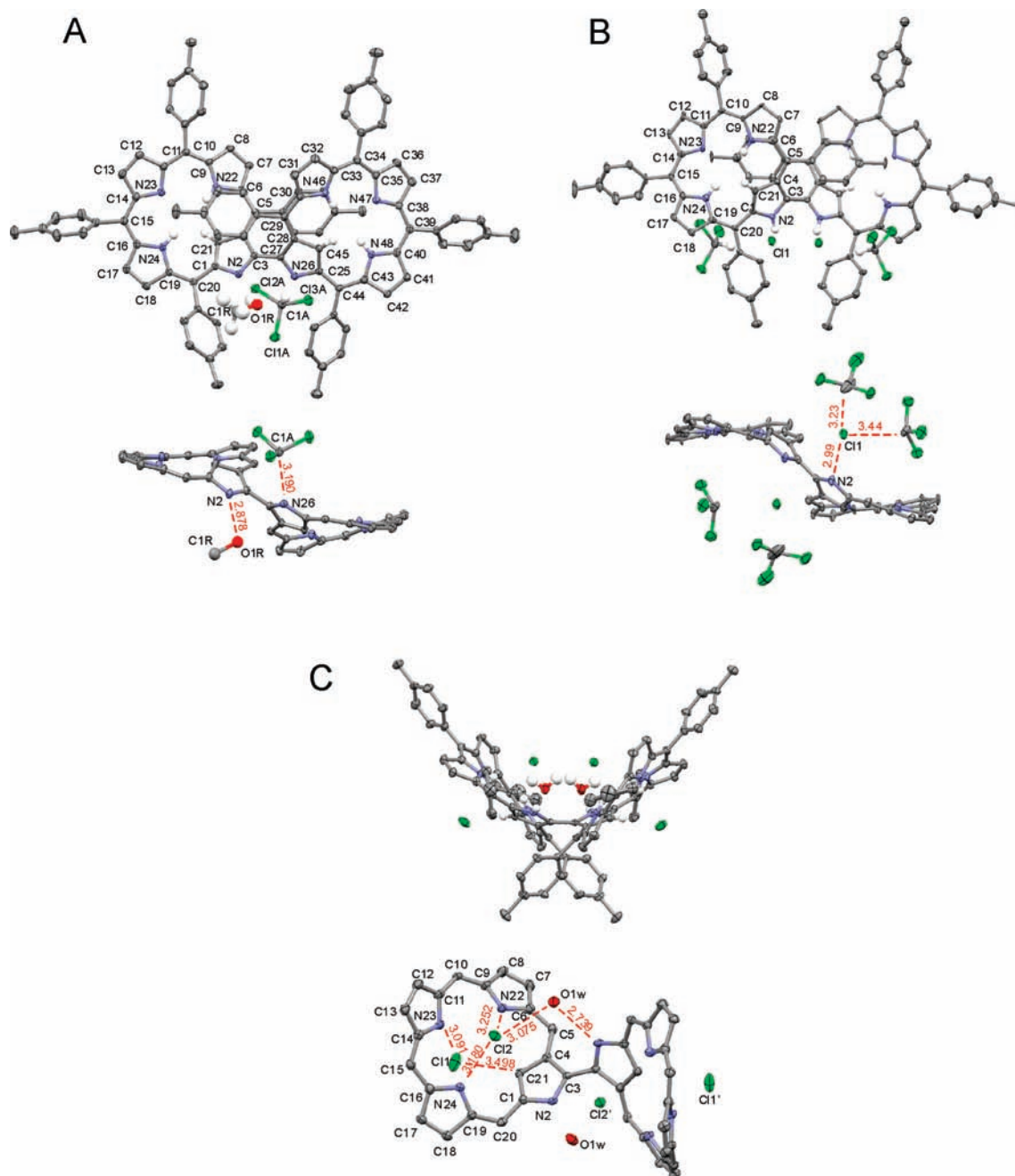
Figure 4. Perspective views of the molecular structures of **2** (A), **2**(HCl)$_2$ (B), and **2**(HCl)$_4$(H$_2$O)$_2$ (C) with thermal ellipsoids set at the 50% probability level and the numbering scheme of the macrocycle ring atoms. Arbitrarily, only the structures of atropo enantiomer M are shown for each form. All hydrogen atoms are omitted except for those located within the macrocyclic rings and on the guests in the upper views. All *meso*-aryl substituents are omitted in the lower views. The distances between hydrogen-bond-forming atoms (in Å) are shown.
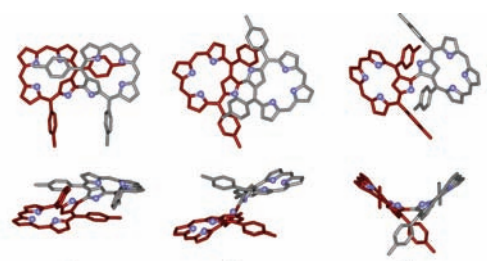
conformer **c**, the TA$_{NCCN}$ torsion angle is about 61° and DA$_{2121}$ is 36.6°, which resemble the structural features observed for this system in the solid state[50] (see also the X-ray data analysis in this paper). The transoid conformer **t** can be formally obtained from the conformer **c** by about a 120° rotation around the C3—C3′ bond with a concurrent change in the direction of the displacement of C21 with respect to the mean plane P$_{21}$ in one of the subunits. In the energy-optimized model of this conformer, the bipyrrole fragment is essentially planar, the TA$_{NCCN}$ torsion angle is 180°, and the mean macrocyclic planes are parallel. Unlike conformer **c**, this transoid conformer is effectively

centrosymmetric and thus achiral consisting of two heterochiral subunits. A rotation of the subunits in **c** around the bridging bond by 180° resulted in a bent structure of chiral transoid conformer **tb** where the torsion angle of the bipyrrole moiety is about −120° but the dihedral angle DA$_{2121}$ between the mean planes P$_{21}$ is close to 90°. A structure of this type had been previously observed in the solid state for the bis(chlorozinc) complex of **2**[51] (see also the X-ray data analysis for the tetracation chloride complex in this paper). It is important to note that because of their chiral character **c** and **tb** are each represented by two energy-degenerated nonsuperimposeable structures that differ in

the sign of TA_{NCCN}. For our calculations, we chose enantiomers P for all conformers **c** (positive sense of TA_{NCCN}) and enantiomers M for all conformers **tb** (negative sense of TA_{NCCN}).

The structural models were optimized starting from these three initial geometries for (n), $(m)^+$, $(d)^{2+}$, and $(q)^{4+}$, i.e., for neutral and mono-, di-, and tetracationic forms of **2**, respectively. The structures along with the relative energies of the conformers at each of the protonation stages are presented in Table 4 (see also Figure S5 in the Supporting Information), and structural features defining the conformers of each form are collected in Table 5 along with the appropriate X-ray data determined for the neutral and di- and tetracationic species.

Table 4. Relative Energies (kcal/mol) of Neutral and Mono-, Di-, and Tetraprotonated Bis(NCP) Calculated for Three DFT-Optimized Structures[a]

	c	t	tb
(n)	1.7	16.2	0
$(m)^+$	0	13.9	1.7
$(d)^{2+}$	0	11.7	3.8
$(q)^{4+}$	9.6	45.8	0

[a] A stick representation of each structure is shown in two projections. All hydrogen atoms are omitted. Nitrogen atoms are marked by blue spheres. Aryl substituents are shown only in positions 5 and 20 of both subunits.

Somewhat surprisingly, the most stable among the neutral conformers appears to be the bent transoid structure despite the observed occurrence of **c**(n) rather than **tb**(n) both in the solid state and in solution, which have been shown by means of the single-crystal X-ray and low-temperature NMR data analyses, respectively. The energy difference, however, is less than 2 kcal/mol, and that result practically indicates an equal availability of both conformations upon a rotational freedom. An advantage of one of the conformers in vitro may be due to some extrinsic contributions to the total energy like solvation or packing forces, which have been omitted in our gas-phase density functional theory (DFT) calculations. The least stable appears to be conformer **t**(n), likely due to the most distorted and then the most strained structure of the subunits. The distortion is reflected by a high value of the dihedral angle DA_{21C} (47° compared to about 30° in other conformers) and strong displacements of *meso*-carbon atoms 5 and 20 from the mean plane P_{21} [0.48 and −0.59 Å, respectively, compared to 0.26 and 0.03 in **c**(n) or 0.17 and 0.19 Å in **tb**(n)]. In fact, the energies of conformers of this type are highest also for the protonated forms from $(m)^+$ to $(q)^{4+}$. In the case of monoprotonated species $(m)^+$, the cisoid conformer is most stable, although, again, the energy difference between $c(m)^+$ and $tb(m)^+$ is small. There is a change in the TA_{NCCN} torsion angle from 62° in **c**(n) to 48° in $c(m)^+$, but otherwise the shapes of the neutral and monoprotonated forms are similar. An additional stabilization of the cisoid and more planar conformations of the bipyrrole fragment due to intramolecular hydrogen bonding could be expected. However, the unfavorable orientation of the nitrogen atoms (the calculated N2—H···N2′ angle is 90°) despite their relatively close distance (2.83 Å) prevents this kind of interaction. The formation of such a hydrogen bond is conceivable only provided that its symmetric character allows for a N···H···N angle of about 125°. The lack of symmetry observed in the ^1H NMR spectrum of the monocation rules out this possibility. The cisoid conformer is also most stable in the case of the dication despite the repulsive contribution

Table 5. Selected Structural Features of the Conformers Calculated for Various Forms of 2 or Derived from X-ray Crystal Structures

form	DA_{2121}[a] [deg]	DA_{21C}[b] [deg]	DA_{CC}[c] [deg]	TA_{NCCN}[d] [deg]	R_{NN}[e] [Å]	source
c(n)	36.6	26.4	60.4	61.6	2.98	DFT
t(n)	0.0	47.1	0.0	180.0	3.63	DFT
tb(n)	88.1	31.7	51.0	−125.2	3.41	DFT
$c(m)^+$	24.7	29.2, 32.1[f]	48.9	47.9	2.83	DFT
$t(m)^+$	4.7	49.9, 50.7[f]	5.5	176.0	3.66	DFT
$tb(m)^+$	87.8	33.4, 35.9[f]	48.5	−128.1	3.46	DFT
$c(d)^{2+}$	23.5	33.9	57.8	57.3	3.01	DFT
$t(d)^{2+}$	16.8	53.2	19.4	162.1	3.69	DFT
$tb(d)^{2+}$	88.2	36.6	46.4	−129.3	3.52	DFT
$c(q)^{4+}$	76.6	30.5, 31.4	80.1	74.2	3.10	DFT
$t(q)^{4+}$	0.0	51.9	0.0	180.0	3.78	DFT
$tb(q)^{4+}$	87.0	40.4	41.1	−134.7	3.56	DFT
2, solid	15.60(4)	33.57(7), 37.45(8)	56.25(9)	−60(3)	2.975(3)	X-ray
$2(HCl)_2$ solid	1.84(8)	45.5(2)	46.1(3)	−49(2)	2.89(1)	X-ray
$2(HCl)_4(H_2O)_2$ solid	83.63(3)	39.6(2)	50.2(2)	−125.2(7)	3.445(6)	X-ray

[a] Dihedral angle between the mean planes of the subunits defined by 21 heavy atoms of the macrocyclic ring (P_{21}) in each of the subunits (all atoms of the macrocyclic ring except for N2, C3, and C21). [b] Dihedral angle between the mean plane of the confused pyrrole and the mean plane of the macrocycle (P_{21}) defined by 21 heavy atoms of the macrocyclic ring (all atoms of the macrocyclic ring except for N2, C3, and C21). [c] Dihedral angle between the mean planes of the *confused* pyrroles. [d] Torsion angle N2—C3—C3′—N2′. [e] Distance between the nitrogen atoms of the bipyrrole moiety. [f] Value for the protonated subunit.
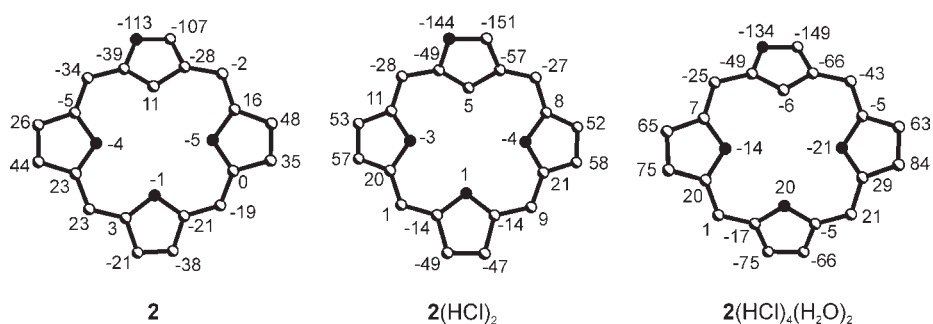
Figure 5. Diagrams showing displacement (in Å × 10^{-2}) of the ring atoms from the mean plane P$_{21}$ defined by all ring atoms except N2, C3, and C21. Nitrogen atoms are marked with filled circles.
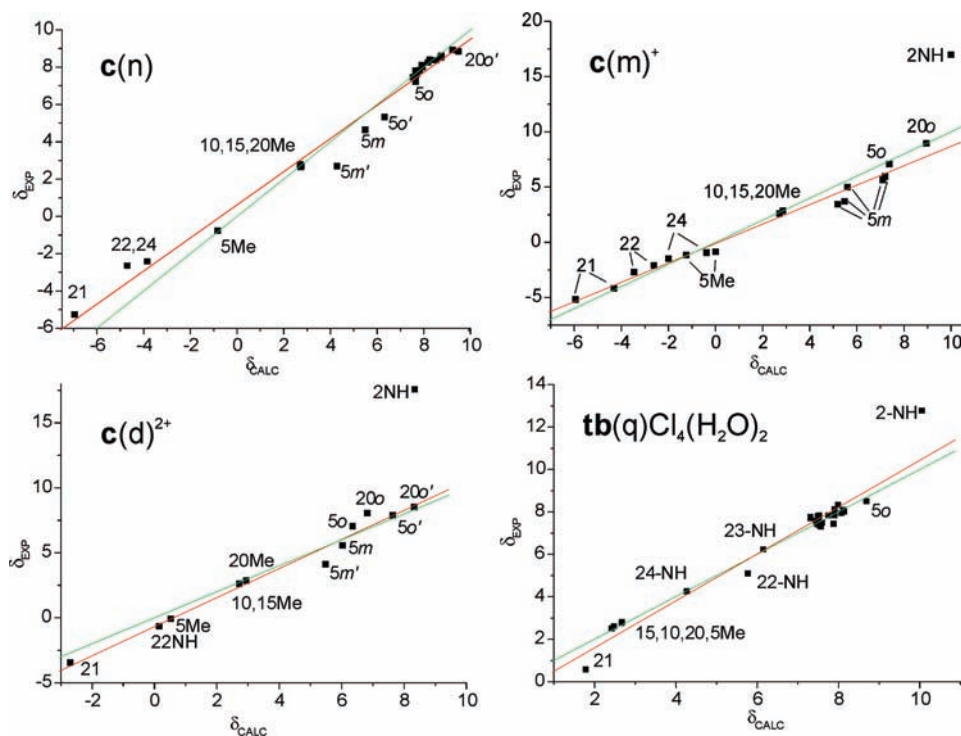

Figure 6. Correlation diagrams of experimental ^{1}H NMR chemical shifts δ_{EXP} of selected protons for the specified forms of **2** (CDCl$_3$, 300 K) vs GIAO-calculated chemical shifts δ_{CALC}. The red lines are calculated on the basis of least-squares fitting to the δ_{EXP} vs δ_{CALC} data sets, and the green lines are traced for the same values on both axes.

of two positively charged NH sites, which apparently are closer to each other in **c**(d)$^{2+}$ than in any of the transoid isomers (see the N2−N2′ distances R_{NN} in Table 5). The TA$_{NCCN}$ torsion angle in **c**(d)$^{2+}$ is 58°, which means a slight increase with respect to that adopted by **c**(m)$^+$ in the energy minimum, but the other structural features remain similar in cisoid mono- and dications. The situation is essentially different in the case of the tetracation, for which the bent transoid conformer **tb**(q)$^{4+}$ is the most stable form with a total energy of about 10 kcal/mol lower than that of the **c**(q)$^{4+}$ and almost 46 kcal/mol lower compared with the energy of **t**(q)$^{4+}$. A stronger saddle-shaped distortion of the tetrapyrrolic rings is clearly due to the presence of four protons inside the macrocyclic crevice in tetracationic forms, which moves "internal" atoms out of the macrocycle's mean plane: C21 and N23 in one direction and N22 and N24 in the other.

For each of the systems, proton NMR chemical shift arrays were obtained by means of the gauge-independent atomic

orbitals (GIAO) approach performed for the DFT-calculated models. The values calculated for each conformer were correlated with experimental chemical shifts of protons in the free base **2** and mono-, di-, and tetracations (Figure S6 in the Supporting Information) assigned on the basis of 2D COSY and NOESY experiments (Figures S4, S7, and S8 in the Supporting Information). In the case of free base, a good agreement between experimental data and those calculated for **c**(n) was obtained for all protons (Figure 6). Similarly, in the case of a mono- or dication, the chemical shifts of all but one proton (exception for 2-NH), which can be unequivocally identified, correlate well with the values calculated for cisoid conformers in line with their highest relative stability (Figure 6).

The most conformation-sensitive resonances are those of the *p*-tolyl substituents in the meso position 5, i.e., protons 5*o*, 5*o*′, 5*m*, 5*m*′, and 5Me (i.e., *p*-methyl group of the tolyl substituent in position 5). In the cisoid conformers, the aryl substituent located
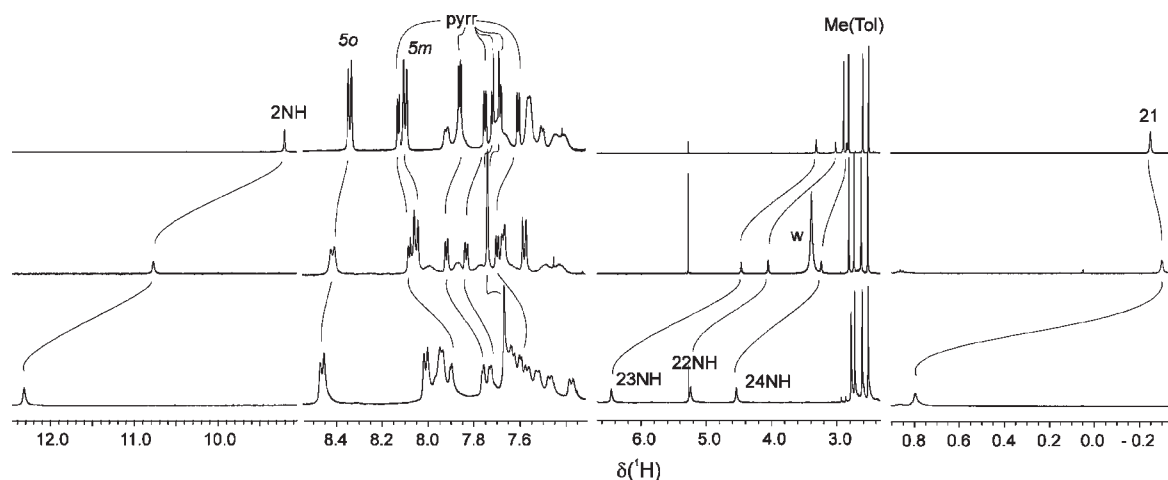
Figure 7. ^{1}H NMR spectra (600 MHz, CDCl$_3$, 300 K) of quadruply protonated **2** associating different anions (from top to bottom): BF$_4^-$, MeSO$_3^-$, Cl$^-$. The curved lines join signals of protons at the same positions in the structure of the host (the labeling follows that of Chart 1; w = signal of dissolved water).

in this position is strongly shielded by the aromatic ring current of the neighboring subunit. Consequently, the signals of these protons are shifted considerably upfield in the neutral and mono- and dicationic forms. This effect is well reproduced by the calculations for the cisoid conformers of each of these forms. No such shielding influence is expected for the transoid or bent transoid conformations. The observed chemical shifts of protons belonging to 5-*p*-Tol do not differ significantly from those of aryls located in the other meso positions. Thus, the formation of tetracation is accompanied by distinct spectral changes consisting of a downfield shift of the internal protons and a lack of shielding influence on 5-*p*-Tol, in line with the bent transoid conformation of this form. Importantly, the through-space proton—proton interactions between 2-NH and aryl protons of the substituents in positions 5 and 20 as well as contacts between protons of these two aryls observed in NOESY and ROESY spectra are consistent with such a formulation of the tetracation's structure in solution (Figures S4, S7, and S8 in the Supporting Information). Conformation of the bis(porphyrinoid) skeleton selectively influences the dynamics of the aryl in position 5. In the cisoid conformer at room temperature, substituents at positions 10, 15, and 20 rotate around their meso—ipso bonds with rates that are fast on the NMR time scale. Such rotation results in a broadening and averaging of the ortho and meta resonances for each substituent, and decoalescence of these signals is observed down to a temperature of about 250 K. In the case of 5-*p*-Tol, the four distinct ring proton signals are observed even at elevated temperatures in (n) and at room temperature in (m)$^+$ and (d)$^{2+}$, which can be accounted for by the lack of rotational freedom due to the situation of the aryl ring in a close distance to the macrocyclic ring of the neighboring subunit in the cisoid conformation. On the other hand, no such restriction for this substituent is observed for the tetracation. In the ^{1}H NMR spectra of (q)$^{4+}$ recorded at room temperature, only one degenerate signal is observed for 5o or 5m protons (Figure S7 in the Supporting Information). This is again in line with the predicted bent transoid conformation of this form.

Strong deviations of the calculated chemical shift values from those observed for 2-NH in a solution of cations can be rationalized as an involvement of this proton in a hydrogen bond with an anion or with a water molecule. The chemical shift

Table 6. Selected Proton Chemical Shifts (CDCl$_3$) of the Tetracationic Form of 2 Complexing Various Anions

anion	T [K]	2-NH	5o	23-NH	22-NH	24-NH	21	guest
				δ [ppm]				
BF$_4^-$	300	9.22	8.35	3.32	3.03	2.85	−0.24	
	213	9.08	8.47	3.09	2.88	2.76	−0.51	
HSO$_4^-$	300	10.15	8.34	4.12	3.44	3.26	−0.61	
Br$^-$	300	12.34	8.43	5.84	5.02	4.35	0.84	
	213	12.91	8.52	5.60	4.80	4.03	0.58	
			8.33					
Cl$^-$	300	12.45	8.48	6.48	5.21	4.53	0.79	
	213	12.79	8.51	6.23	5.09	4.27	0.58	
			8.32					
NO$_3^-$	213	10.88	8.47	4.97	4.40	4.07	−0.51	
			8.31					
TFA$^-$	300	11.10	8.39	5.78	5.09	4.47	−0.02	
	213	11.61	8.46	6.00	5.52	4.30	−0.04	
			8.36					
DCA$^-$	213	11.71	8.53	6.39	6.13	4.39	0.06	
			8.26					
								4.21[a]
								3.09[b]
MeSO$_3^-$	300	10.79	8.41	4.48	4.07	3.24	−0.29	1.53[c]

[a] Signal of CCl$_2$HCOO$^-$ bound outside the host's cleft. [b] Signal of CCl$_2$HCOO$^-$ bound inside the host's cleft. [c] Signal of CH$_3$SO$_3^-$.

calculated for the DFT-optimized model of **c**(d)$^{2+}$ with chloride located within the hydrogen-bond distance to each of the protonated external nitrogen atoms (N2—Cl distance 3.0 Å, N2—H···Cl angle 135°) is closer to the experimental results obtained for a dication upon titration of **2** with HCl (δ_{EXP} = 15.8 ppm) than those obtained for **c**(d)$^{2+}$ without the guest. The δ_{CALC} = 12.0 ppm for 2-NH is considerably shifted downfield with respect to the value calculated for the system without chloride (δ_{CALC} = 8.2 ppm). Also, in the case of tetracation calculation of the chemical shifts performed for the model comprising four chlorides localized pairwise on the opposite
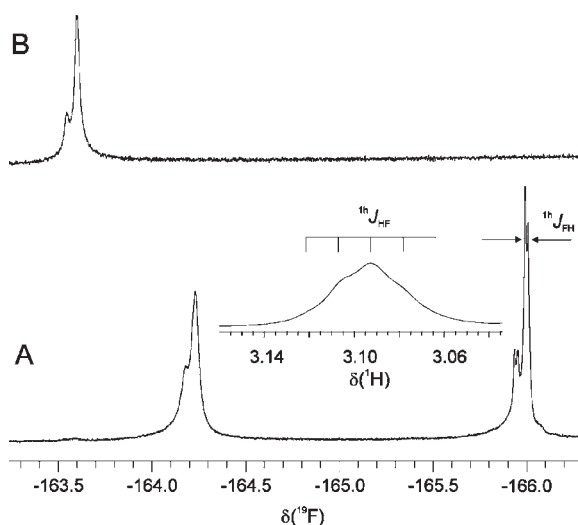
Figure 8. ^{19}F NMR spectra (470 MHz, $CDCl_3$, 213 K) of $(q)(BF_4)_4$ (A) and $(q)Cl_4$ (B) obtained by the addition of 5 equiv of chloride to the former sample. The inset in part A presents an extension of a fragment of the ^1H NMR spectrum (500 MHz, $CDCl_3$, 213 K) of $(q)(BF_4)_4$ consisting of a 23-NH signal with splitting due to the proton coupling with four fluorine nuclei marked with sticks. The splitting of the same constant (7.5 Hz) can be observed in the ^{19}F NMR spectrum on the lines of both ^{11}B and ^{10}B isotopomers of the BF_4^- ions interacting with 23-NH.

Figure 9. Dependencies of absorbance at the specified wavelengths on the equilibrium concentration of chloride upon spectrophotometric titration of $(q)(BF_4)_4$ with $[BzEt_3N]Cl$ (298 K, chloroform). Solid lines were calculated on the basis of a nonlinear least-squares fitting procedure, assuming the presence of two consecutive 2:1 equilibria ($K_{e2} = 3 \times 10^{10}$ M^{-2}; $K_{e4} = 1 \times 10^9$ M^{-2}). In the inset, the dependence of absorbance at 592 nm on the chloride/$(q)(BF_4)_4$ molar ratio is shown along with construction indicating an overall stoichiometry of 4:1 for the anion exchange.

faces of each of the subunits and hydrogen-bonded to the internal nitrogen atoms, the results match satisfactorily the experimental values of protons 22, 23, and 24 measured for the $(q)Cl_4$ system, i.e., the fully protonated **2** obtained by means of HCl (Figure 6). An improvement of the fit for 2-NH in this system is observed for the model with a water molecule placed nearby each of the external nitrogen atoms (N2−O distance 2.78 Å, N2−H···O angle 157°). The calculated value of the chemical shift for this proton in $\mathbf{tb}(q)Cl_4(H_2O)_2$ is $\delta_{CALC} = 10.0$ ppm ($\delta_{EXP} = 12.8$ ppm), while for $\mathbf{tb}(q)^{4+}$ without associated water and anions, $\delta_{CALC} = 6.4$ ppm. Thus, the structural features observed in the solid state for the tetracation, that is, the bent transoid conformation and association of anions and water molecules, are clearly retained in solution.

Anion Binding. The differences in both the optical and ^1H NMR spectral properties observed among protonated systems obtained by means of various acids indicate specific interaction with anions in solution (Figure 7). A variety of anion complexes with the quadruply protonated system $(q)^{4+}$ can be obtained by the combination of a chloroform solution of **2** with a water solution of strong mineral acid (e.g., HBF_4, HCl, HBr). Some of the organic acids can be added in a controlled manner, allowing observation of complexes of mono- and dicationic species as well. Alternatively, a complex with one type of anion can be converted into another by the addition of an appropriate tetraalkylammonium salt in a homogeneous way, which allows spectroscopic monitoring of the guest exchange. Table 6 presents selection of the chemical shifts for several complexes of tetracation with various anions.

Apparently, the spectral responses of protons that are located inside the macrocyclic crevice are most sensitive to the differences of the anion properties, which can be accounted for by the character of the host−guest interaction as well as by the location of anions in the complex. The formation of hydrogen bonds with
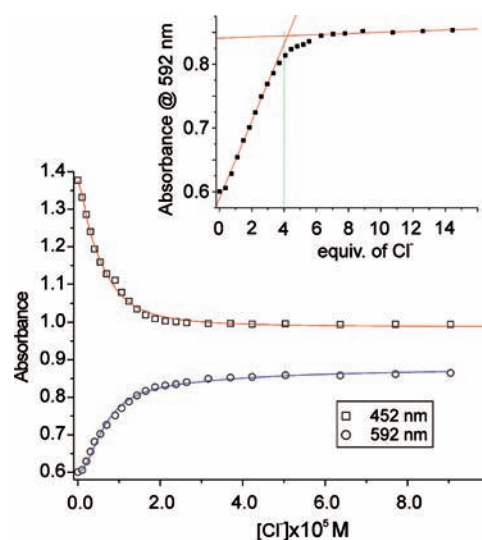
anions shifts the signals of internal NH downfield; thus, the system with tetrafluoroborate anions giving the least shifted NH signals can be considered as the one of weakest bound anions. There is, nevertheless, direct evidence for the hydrogen bonding of BF_4^- to $(q)^{4+}$ in solution. A quintet structure of 23-NH observed at 213 K in the ^1H NMR spectrum of $(q)(BF_4)_4$ in $CDCl_3$ (Figure 8), although ill-resolved, strongly suggests interaction of this proton with four ^{19}F nuclei ($^{1h}J_{HF} = 7.5$ Hz). The ^{19}F NMR spectrum recorded under the same conditions (Figure 8) reveals the presence of two signals of tetrafluoroborate at δ_F −164.24 and −166.02 (data for the more populated $^{11}BF_4^-$), and the latter peak has a doublet structure due to the spin−spin interaction with one proton ($^{1h}J_{FH} = 7.5$ Hz). The chemical shifts of these signals differ by about 1.8 ppm, and none of them represents an "unbound" anion, which can be established by referring to the spectra of tetrabutylammonium tetrafluoroborate, where the signal of $^{11}BF_4^-$ appears at δ_F −163.0 ($CDCl_3$, 213 K). After substitution of BF_4^- with chloride (vide infra), there is only one signal in the ^{19}F NMR spectrum at δ_F −163.6, that is, shifted downfield with respect to those of the bound anions. The differentiation of the chemical shifts as well as different multiplicities of the signals in $(q)(BF_4)_4$ reflects various positions and interactions between $(q)^{4+}$ and the anions. The more upfield-shifted doublet represents two equivalent anions that are located outside the cleft of the host as they interact with the favorably oriented 23-NH, while the other signal is that of the anions interacting with 22- and 24-NH, which point toward the interior of the cleft. At room temperature, there is only one very broad signal ($\Delta\nu_{1/2} = 760$ Hz) centered at −150 ppm in the ^{19}F NMR spectrum of $(q)(BF_4)_4$, clearly indicating fast exchange between binding sites.

^{19}F NMR of the tetracationic system with trifluoroacetate $(q)(TFA)_4$ also indicates anion binding in two different sites.
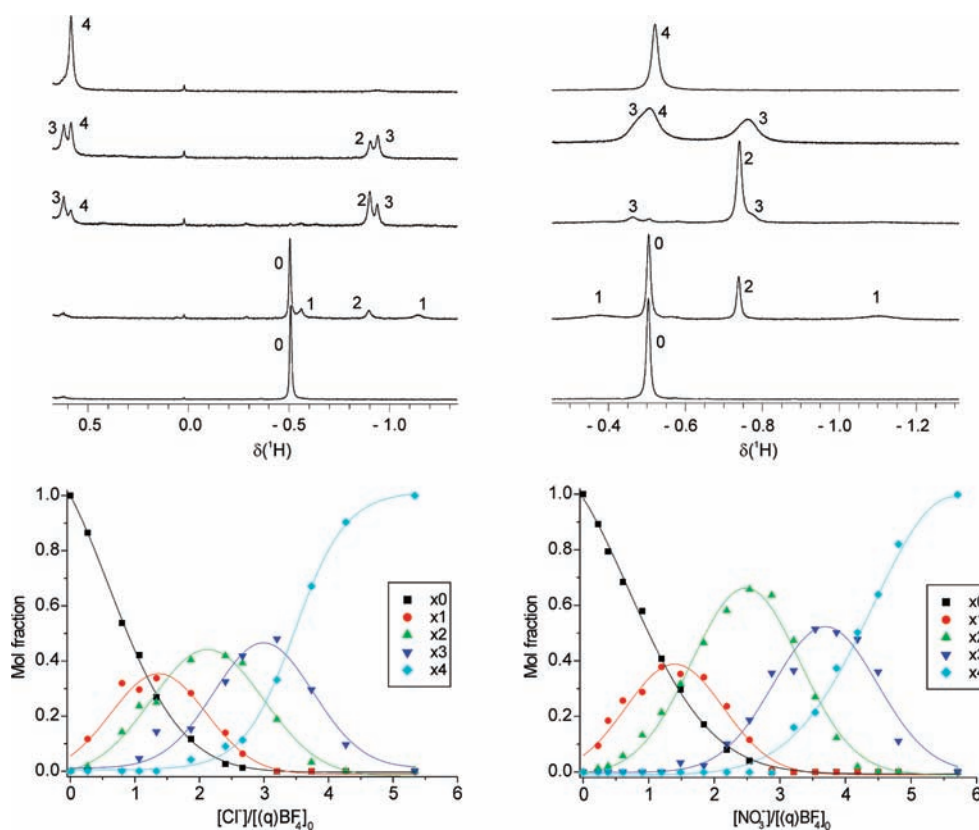
Figure 10. Speciation of complexes of composition $(q)(BF_4)_{4-n}(A)_n$ $(A = Cl^-, NO_3^-)$ formed upon titration of $(q)(BF_4)_4$ with $[BzEt_3N]Cl$ (left) and $[Bu_4N]NO_3$ (right). Data are based on the integration of deconvoluted signals of 21-CH observed in ^1H NMR spectra ($CDCl_3$, 213 K). Selections of the fragments of the spectra taken near the maximum contribution of each form are presented for both systems in the upper graphs. The number associated with the signal indicates the composition of the complex.

At 213 K for the $CDCl_3$ solution of **2** containing 4 equiv of TFAH, there are two sharp equally intense signals of the CF_3 group observed at δ_F −75.98 and −78.81, while in the spectrum of free acid recorded under the same concentration and temperature conditions, the signal appears at δ_F −75.86. A coalescence of the resonances is observed at 283 K, and at room temperature, there is one sharp signal at δ_F −76.93. The addition of 6 equiv of CF_3COOH to the solution of **2** results in the observation of three signals at 213 K (δ_F −76.00, −76.55, and −78.83). This suggests that un-ionized acid is able to interact with the quadruply protonated **2**, apart from two pairs of magnetically inequivalent TFA$^-$ anions (see Figure S9 in the Supporting Information).

The ^1H NMR spectrum at 213 K of the tetracation complex with dichloroacetate $(q)(DCA)_4$ also reveals the presence of two types of inequivalent anions. The signals of the $CHCl_2$ group are strongly shifted upfield with respect to the signal of free acid (δ_H 6.0), which is in line with the shielding effect of the aromatic ring current of the porphyrinoid (Table 6). Integral intensities of these signals indicate the presence of one anion of each type per NCP subunit and, thus, four DCA$^-$ anions in the dimer. The NOESY and ROESY experiments indicate through-space interactions of DCAs' protons with different β-pyrrole protons of the host: the proton resonating at δ 4.21 interacts with protons 7, 8, 17, and 18, while that of δ 3.09 correlates with 12 and 13. Considering saddle-shaped distortion of the macrocycle rings, observed in the solid state or predicted by modeling for the tetracation (Figures 4 and 5), such a correlation pattern locates the more upfield resonating
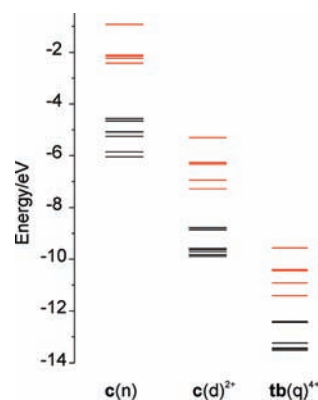
Figure 11. Energy levels of selected orbitals calculated for neutral **2** $[c(n)]$, dication $[c(d)^{2+}]$, and tetracation $[tb(q)^{4+}]$ forms. The energy levels of the virtual orbitals are drawn in red.

anion inside, and the other outside, the cleft formed by the dimer. These experiments indicate also a chemical exchange between the anions in the binding sites located inside and outside the cleft.

It should be noted that when the acid concentration exceeds 4 equiv, another signal appears at δ_H 4.86 and its intensity increases with the concentration of $CHCl_2COOH$. We assigned this peak to the $CHCl_2$ group of the un-ionized acid molecule on the basis of NOESY and ROESY spectra, where chemical

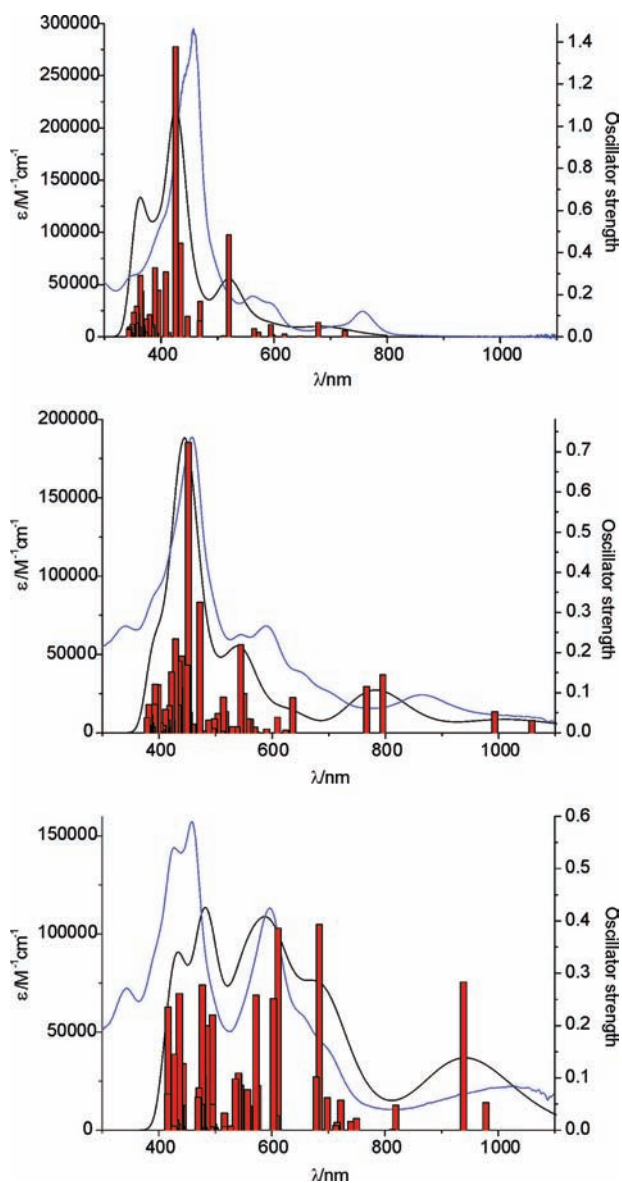**Figure 12.** Electronic transitions (red sticks) and spectra (black lines) calculated by means of TDDFT for $\mathbf{c}(n)$ (top), $\mathbf{c}(d)^{2+}$ (middle), and $\mathbf{tb}(q)^{4+}$ (bottom). The experimental dichloromethane spectra of **2**, **2**(TFAH)$_2$, and **2**(TFAH)$_4$, respectively, are superimposed as blue traces.

exchange correlations of this proton with those of both chloroacetate anions are observed. The acid molecule clearly interacts with the system consisting of host $(q)^{4+}$ and four anions DCA$^-$ because the resonance frequency of its signal is considerably shifted upfield with respect to the unbound acid. The presence of the acid excess causes also a line broadening that is characteristic for dynamic systems. Similar effects are observed at 213 K for several other carboxylates including TFAH (vide supra) and for methanesulfonic acid. That kind of interaction with "surplus" acid molecules has been observed recently in the solid state and in solution for the expanded benziporphyrins of flexible topology.[56] Crystallization with three un-ionized molecules of acetic acids, apart from two hydrogen-bonded acetates, has also been reported for a heavily distorted dication of the tetrapyrrolic system.[28]
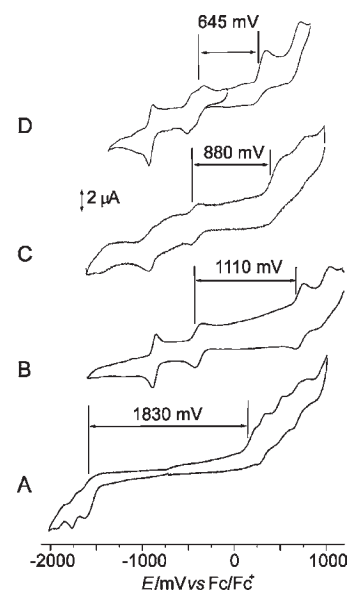

Figure 13. Cyclic voltammograms (CH$_2$Cl$_2$, supporting electrolyte [Bu$_4$N]BF$_4$) of **2** (A), **2**(HBF$_4$)$_4$ (B), **2**(HCl)$_4$ (C), and **2**(HBr)$_4$ (D). The values of the differences between the first reduction and first oxidation potentials are associated with traces for each system.

Although the NH resonances are most responsive to the type of anion interacting with $(q)^{4+}$, the significant differences in the chemical shifts among the systems are observed for other protons that apparently do not participate in the hydrogen bonding (Figure 7 and Table 6). Interaction with anions also strongly affects the ^{13}C NMR spectral parameters, resulting in a differentiation of the resonance positions among the tetracations obtained with various acids (Figure S10 in the Supporting Information); for instance, signals of C21 appear at 86.2, 90.2, and 95.2 ppm (CDCl$_3$, 300 K) for HBF$_4$, MeSO$_3$H, and HCl as a proton supplier, respectively. This suggests that the presence of anions inside the cleft of the tetracation introduces fine modifications to the bent transoid structure of the bis(NCP) skeleton (e.g., dihedral angles DA$_{2121}$ or DA$_{21C}$), and thus complexes differ in the electron density distribution onto the particular fragments and/or in the aromatic ring current effect.

Anion Exchange. The substitution of anions can be followed by both optical and NMR spectroscopic techniques. The complex with tetrafluoroborate anion $(q)(BF_4)_4$ appears to be the most suitable to explore this process because of its relatively weak interaction with the host. Alterations of the UV−vis spectra observed upon the addition of tetraalkylammonium salts of other anions ([BzEt$_3$N]Cl, [Bu$_4$N]Br, and [Bu$_4$N]HSO$_4$) to the solution of $(q)(BF_4)_4$ at room temperature indicate exchange of the anion interacting with $(q)^{4+}$. A total 4:1 stoichiometry of the reaction can be established on the basis of such a titration; however, the spectral alterations seem not to be sufficiently diagnostic to show the formation of intermediates, i.e., mixed-anion complexes. Nevertheless, we rationalize the absorbance dependences on the incoming anion concentration in terms of two consecutive 2:1 equilibria (Figure 9). The first equilibrium constant K_{e2} is about 2 orders of magnitude higher than the second constant K_{e4} ($K_{e2} = 6 \times 10^{10}\,M^{-2}$ and $K_{e4} = 2 \times 10^9\,M^{-2}$ for chloride and $K_{e2} = 2 \times 10^{10}\,M^{-2}$ and $K_{e4} = 2 \times 10^7\,M^{-2}$ for bromide; the estimation errors are less than 15%). We performed similar experiments of anion exchange for the system consisting

Table 7. Electrochemical Data for 2 and Its Tetracation Complexes

	E_{red}^1 (ΔE_{ac}) [mV]	E_{red}^2 (ΔE_{ac}) [mV]	E_{ox}^1 (ΔE_{ac}) [mV]	E_{ox}^2 (ΔE_{ac}) [mV]	E_{ox}^3 (ΔE_{ac}) [mV]	E_{ox}^4 (ΔE_{ac}) [mV]
2	−1610 (60)	−1750 (60)	220[a]	300 (63)	480 (60)	680 (58)
2(HBF$_4$)$_4$	−380 (67)	−870 (29)	730 (80)	1000 (85)		
2(HCl)$_4$	−420 (70)	−900 (40)	460 (100)	730 (60)		
2(HBr)$_4$	−340 (80), −465 (60)	−895 (35)	305[a]	700 (90)		

[a] The oxidation peak potential of an irreversible wave.

of **2** acidified with a 10-fold excess of TFAH. In this case, titrations with chloride, bromide, hydrogen sulfate, or perchlorate give results similar to those obtained for the tetrafluoroborate complex. Apparently, there is no particular preference of the system for any of these anions, although these experiments reveal that trifluoroacetate or tetrafluoroborate can be easily substituted by other anions. On the other hand, (q)Cl$_4$ does not convert to (q)(BF$_4$)$_4$ even upon the addition of 1000 equiv of [Bu$_4$N]BF$_4$. In some instances ([Bu$_4$N]H$_2$PO$_4$, [Bu$_4$N]F), titration of the tetracation complex with the salt results in a gradual deprotonation and conversion to the dication. It may be due to a lower basicity of the internal protonation sites in comparison with that of the incoming anions. In fact, our efforts to obtain tetracations from **2** and water solutions of H$_3$PO$_4$ or HF failed to result in stable complexes.

The formation of mixed-anion complexes, i.e., systems consisting of tetrafluoroborate and the other anion bound to the tetracation, can be observed by an ^{1}H NMR-monitored titration of (q)(BF$_4$)$_4$ with tetraalkylkammonium salts at low temperature (213 K, CDCl$_3$). Two asymmetric and one symmetric adducts are formed upon a stepwise addition of chloride or nitrate to the solution of (q)(BF$_4$)$_4$, and the spectrum of the final product represents (q)Cl$_4$ or (q)(NO$_3$)$_4$, respectively. The composition of intermediates can be logically described as (q)(BF$_4$)$_{4-n}$Cl$_n$ or (q)(BF$_4$)$_{4-n}$(NO$_3$)$_n$. The asymmetric character of the complexes with n = 1 or 3 implies substitution of the anion in one or three binding sites and a slow exchange rate between the sites on the ^{1}H NMR time scale. The 21-CH peaks located in the high-field part of the spectrum are most suitable to follow the process of anion exchange, and contribution of each of the components can be established on the basis of the signal integration (Figure 10). Although none of the intermediates can be observed as a unique species in solution, the sequential increase and/or decrease of the mole fraction of each form clearly indicates a consecutive character of the anion-exchange equilibria. Also, an evolution of the ^{19}F NMR spectral response of (q)(BF$_4$)$_4$ upon the addition of chloride (CDCl$_3$, 213 K) indicates involvement of this anion in the substitution process. However, the equilibria are within a fast exchange limit for ^{19}F and only a severe line broadening and shift of an averaged signal can be observed rather than the simultaneous presence of the consecutive intermediates upon an increase in the chloride concentration. After the addition of 5 equiv of chloride, the signal of BF$_4^-$ becomes sharp (Figure 8), but its chemical shift (δ_F −163.6) is still lower than that of the unbound tetrafluoroborate and can be further changed by the chloride concentration increase.

Electronic Properties. The electronic structures of neutral and cationic forms of **2** were analyzed by means of time-dependent DFT (TDDFT) calculations performed for the DFT-optimized structures of **c**(n), **c**(d)$^{2+}$, and **tb**(q)$^{4+}$. A prominent decrease of the HOMO−LUMO gap (HLG) from 2.14 eV in the free base **c**(n) to 1.50 eV in the dication **c**(d)$^{2+}$ and

to 1.00 eV in the tetracation **tb**(q)$^{4+}$ and a low-energy shift of the frontier orbitals (Figure 11) were established. Electronic spectra calculated for 45, 55, and 60 transitions in the case of **c**(n), **c**(d)$^{2+}$, and **tb**(q)$^{4+}$, respectively, reasonably reproduce the experimental spectra of the respective forms in the region of 400−1100 nm, although calculated transition frequencies tend to deviate systematically from those observed in the direction of higher values for neutral and dicationic forms (Tables S2−S4 in the Supporting Information and Figure 12). The calculated reduction of HLG is in line with the appearance of the low-energy bands near 900 nm in the case of the dication. Also, a decrease of the intensity and a splitting of the band in the visible region of the optical response of tetracations are similar in the experimental and calculated spectra. On the other hand, calculations for **tb**(q)$^{4+}$ predict allowed near-IR transitions at 1672 and 1660 nm (HOMO → LUMO and HOMO−1 → LUMO transitions), but no band is observed in the experimental spectra of the tetra-cationic species in this region up to 2200 nm.

Changes in the redox properties upon protonation also reflect alteration of the electronic structure of bis(NCP). The cyclic voltammogram of **2** in dichloromethane (Figure 13) consists of two groups of irreversible or quasi-reversible waves: those at the negative potentials are due to one- and two-electron reduction of the system, while the four waves located in the region of $V > 0$ can be assigned to consecutive oxidations resulting in mono-, di, tri, and tetracation radicals (Table 7). In the case of quadruply protonated species, the strong anodic shifts of all redox waves indicate relative stabilization of reduced forms and destabilization of oxidized forms, which is expected considering the highly positively charged character of (q)$^{4+}$. A significant decrease in the separation of the first oxidation and first reduction couples by 720 mV in the case of (q)(BF$_4$)$_4$ with respect to that observed for the free base **2** is in line with calculations predicting a 1.14 eV decrease of the HLG upon going from (n) to (q)$^{4+}$. The absolute value of $E_{ox}^1 - E_{red}^1 = 1110$ mV for (q)(BF$_4$)$_4$ is consistent with the calculated HLG value (1.00 eV). For systems comprising chloride or bromide associated with the tetracation, the second oxidation at a potential of about 700 mV can be assigned to electron removal from the bis(porphyrin) system. The first oxidation waves at 460 and 305 mV in the case of chloride and bromide complexes, respectively, are likely due to Cl$^-$ or Br$^-$ rather than the macrocyclic ring oxidation because at similar potentials appear couples in the cyclic voltammograms of [BzEt$_3$N]Cl or [Bu$_4$N]Br recorded under identical conditions (dichloromethane and [Bu$_4$N]BF$_4$ as supporting electrolytes). Thus, it appears that the HLG or electron donor−acceptor energy separation can be further diminished by binding of an easily oxidizable anion to (q)$^{4+}$. The systems of very small HLG are desirable targets for further physical studies and electronics applications.[57] In the cases of some recently reported fused porphyrins with extended π-orbital systems,[58,59] the small HLG is connected with considerably low oxidation potentials

6732

dx.doi.org/10.1021/ic200742d |*Inorg. Chem.* 2011, 50, 6719–6736

(e.g., $E_{ox}^{1} = -0.44$ V for fused tetraanthracenylporphyrin), which may cause some problems because of its potential reactivity toward atmospheric oxygen. An advantageous feature of the tetraprotonated **2** may be that the major contribution of a decrease of the HLG is due to its unusually high reduction potential and, thus, a potentially useful material would be stable on air. Apparently, reduction and oxidation processes took place simultaneously and independently at both subunits of bis(NCP) in the case of $(q)(BF_4)_4$, unlike in $(q)(Br)_4$, for which the first reduction wave is split into two couples separated by about 120 mV. An electrostatic interaction between the subunits is likely responsible for this splitting. The small peak-to-peak potential difference ($\Delta E_{ac} < 57$ mV) of the second reduction waves at a potential of about -900 mV is in line with the two-electron character of this process. In general, it seems that interaction between the subunits of the tetracation is less pronounced than in the case of a neutral bis(NCP) free base or its complexes with nickel(II)[50] or silver(III)[52] for which differentiation of both the oxidation and reduction potentials of the subunits has been observed. The spatial arrangement of the subunits in the tetra-cation, that is, the bent transoid structure, apparently disfavors electronic and electrostatic interactions between them.

■ CONCLUSION

The protonation of bis(NCP) proceeds in three discrete steps. The external basic sites accept protons consecutively, while both internal sites are protonated in a concerted manner. The nitrogen atoms located on the perimeters of both subunits are significantly more nucleophilic than those of the macrocyclic interiors; thus, the external coordination of the metal ions can always be considered as a first step of the complex formation. The effectiveness of the proton attachment is shown to depend not only on the position of the protonation target but also on the acidity of the proton source. In both the solid state and solution, the protonated species interact with anions and un-ionized acid or water molecules. The stable complexes with anions, however, are formed only for the strong mineral acids. The attachment of four protons triggers a considerable alteration of both the electronic structure of the system and the spatial arrangement of the bis(porphyrinoid) skeleton. That results in significant changes of the spectral and redox properties, which can be potentially applied in the production of dynamic cation- and anion-responding systems. Interaction of protonated $(NCP)_2$ with chiral anions and molecules is an attractive subject considering the intrinsic axial chirality of this system, which, however, displays some adaptability.[51,53] The results of our further study on the systems consisting of this molecular motif will be published in the near future.

■ EXPERIMENTAL SECTION

Instrumentation. The optical spectra were recorded on a Varian Cary 50 Bio spectrophotometer with a Peltier temperature controller in dichloromethane or chloroform. The NMR spectra were recorded in $CDCl_3$ or CD_2Cl_2 on a Bruker 600 MHz Avance III or Bruker 500 MHz Avance II spectrometer equipped with variable-temperature units. 2D experiments (COSY, HMQC, HMBC) were performed by means of standard Bruker software. The low-temperature NOESY spectra were recorded with 2048 × 512 data blocks and with 400 ms mixing time. Signals in the ^{19}F NMR spectra were calibrated with C_6F_6 as an external reference (δ −163). Cyclic voltammetric measurements were performed in dichloromethane on an EA9C MTM apparatus with a glassy

carbon disk as the working electrode, Ag/AgCl as the reference electrode (the ferrocene reference potential was 530 mV), and a platinum wire as the auxiliary electrode. Tetrabutylammonium tetrafluoroborate (0.1 M) was used as the supporting electrolyte.

Syntheses of Starting Compounds. 1 and **2** were obtained by previously described methods,[50,60] and their purity was checked by means of ^{1}H NMR and optical spectra.

General Procedure for the Synthesis of 2(HX)₄(H₂O)₂. A solution containing 10 mg of **2** in chloroform (3 mL) was vigorously shaken for 5 min with 0.5 mL of a concentrated water solution of an acid HX (X = BF_4^-, Cl^-, Br^-, $CH_3SO_3^-$). The organic layer was then separated from the acid solution and layered with equal volumes of hexane. The precipitated dark-green product was collected on the dense sintered glass filter, washed with hexane, and dried on air. Yield: 80−90%.

Selected Data for **2**$(HBF_4)_4(H_2O)_2$. ^{1}H NMR (600 MHz, $CDCl_3$, 300 K): δ_H 9.21 (s, 2H, 2-NH), 8.34 (d, $^3J = 6.8$ Hz, 4H, 5o), 8.12 (dd, $^3J = 5.0$ Hz, $^4J = 1.4$ Hz, 2H, 7), 8.09 (d, $^3J = 6.8$ Hz, 4H, 5m), 7.92 (d, $^3J = 7.0$ Hz, 2H), 7.86 (dd, $^3J = 5.0$ Hz, $^4J = 1.3$ Hz, 2H, 18), 7.85 (b, 1H), 7.75 (dd, $^3J = 5.0$ Hz, $^4J = 1.4$ Hz, 2H, 8), 7.71 (dd, $^3J = 4.8$ Hz, $^4J = 0.9$ Hz, 2H, 13), 7.70 (b, 2H), 7.68 (dd, $^3J = 4.8$ Hz, $^4J = 1.0$ Hz, 2H, 12), 7.66 (b, 2H), 7.60 (dd, $^3J = 5.0$ Hz, $^4J = 1.4$ Hz, 2H, 17), 7.56 (d, $^3J = 6.7$ Hz, 4H), 7.50 (d, $^3J = 6.7$ Hz, 2H), 7.44 (b, 4H), 7.40 (b, 4H), 3.31 (b, 2H, 23-NH), 3.02 (b, 2H, 22-NH), 2.90 (s, 6H, 5-Me(Tol)), 2.84 (b, 2H, 24-NH), 2.82 (s, 6H, 20-Me(Tol)), 2.61 (s, 6H, 10-Me(Tol)), 2.51 (s, 6H, 15-Me(Tol)), 1.41 (b, dissolved water signal), −0.25 (s, 2H, 21). ^{1}H NMR (600 MHz, $CDCl_3$, 213 K): δ_H 9.08 (b, 2H, 2H, 2-NH), 8.47 (d, $^3J = 7.5$ Hz, 2H, 5o), 8.29 (d, $^3J = 7.8$ Hz, 2H, 5o'), 8.20 (d, $^3J = 8.0$ Hz, 2H, 5m), 8.19 (d, $^3J = 8.1$ Hz, 5m'), 8.15 (d, $^3J = 5.0$ Hz, 2H, 7), 8.11 (d, $^3J = 7.3$ Hz, 2H, 10o), 7.97 (d, $^3J = 7.5$ Hz, 2H, 20m'), 7.90 (d, $^3J = 5.0$ Hz, 2H, 18), 7.87 (d, $^3J = 8.2$, Hz, 2H, 15o), 7.84 (d, $^3J = 7.3$ Hz, 2H, 20o), 7.83 (d, $^3J = 5.0$ Hz, 2H, 8), 7.78 (d, $^3J = 7.3$ Hz, 2H, 10o'), 7.75 (d, $^3J = 4.6$ Hz, 2H, 13), 7.74 (d, $^3J = 4.6$ Hz, 2H, 12), 7.63 (d, $^3J = 5.0$ Hz, 2H, 17), 7.59 (d, $^3J = 8.3$ Hz, 2H, 10m), 7.57 (d, $^3J = 7.8$ Hz, 2H, 20m), 7.55 (d, $^3J = 8.3$ Hz, 2H, 15o'), 7.48 (d, $^3J = 7.3$ Hz, 2H, 10m'), 7.46 (d, $^3J = 8.3$ Hz, 2H, 15m), 7.38 (d, $^3J = 8.3$ Hz, 2H, 15m'), 7.35 (d, $^3J = 7.5$ Hz, 2H, 20o'), 3.10 (m, $^{1h}J_{HF} = 7.5$ Hz, 2H, 23-NH), 2.93 (s, 6H, 5Me(Tol)), 2.88 (b. 2H, 22-NH), 2.84 (s, 6H, 20Me(Tol)), 2.77 (b, 2H, 24-NH), 2.59 (s, 6H, 10Me(Tol)), 2.50 (s, 6H, 15Me(Tol)), 0.44 (b, 4H, associated H_2O), −0.50 (s, 2H, 21). ^{19}F NMR (470 MHz, $CDCl_3$, 213 K): δ_F −164.19 (s, $^{10}BF_4$ internal), −164.24 (s, $^{11}BF_4$ internal), −165.96 (d, $^{1h}J_{FH} = 7.5$ Hz, $^{10}BF_4$ external), −166.02 (d, $^{1h}J_{FH} = 7.5$ Hz, $^{11}BF_4$ external). ^{13}C NMR (150 MHz, $CDCl_3$, 300 K): δ_C 154.6, 152.4, 150.0, 148.9, 145.1, 143.5, 143.1, 140.2, 140.1, 138.6, 137.2, 137.0, 135.8, 135.7, 135.5, 135.47, 135.4, 135.2, 134.6, 134.5, 133.1, 133.0, 132.3, 129.7, 129.66, 129.2, 129.17, 129.1, 128.8, 128.7, 128.2, 118.3, 117.8, 86.2 (21-C), 22.2, 22.1, 21.5, 21.4. UV−vis−near-IR ($CHCl_3$, 298 K): λ/nm (ε/$M^{-1}\cdot cm^{-1}$) 350 (74 200), 428 (sh), 457 (191 000), 594 (82 400), 661 (sh), 699 (sh), 976 (23 900). Anal. Calcd (found) for $C_{103}H_{89}B_4Cl_{21}F_{16}N_8O_2$: C, 48.28 (48.74); H, 3.50 (3.83); N, 4.37 (4.11).

Selected Data for **2**$(HCl)_4(H_2O)_2$. ^{1}H NMR (600 MHz, $CDCl_3$, 300 K): δ_H 2.43 (b, 2H, 2-NH), 8.47 (d, $J = 7.8$ Hz, 4H, 5o), 8.00 (d, $J = 7.8$ Hz, 4H, 5m), 7.96 (d, $J = 7.9$ Hz, 2H, 10o), 7.94 (d, $J = 7.6$ Hz, 2H), 7.93 (d, $J = 7.8$ Hz, 2H), 7.90 (b, 2H), 7.88 (d, $J = 4.5$ Hz, 2H, 7), 7.75 (d, $J = 4.6$ Hz, 2H, 18), 7.73 (d, $J = 4.6$ Hz, 2H, 8), 7.70 (b, 2H), 7.67 (d, $J = 4.8$ Hz, 2H, 12), 7.66 (d, $J = 4.8$ Hz, 2H, 13), 7.62 (d, $J = 7.8$ Hz, 2H), 7.59 (d, $J = 4.5$ Hz, 2H, 17), 7.56 (d, $J = 7.2$ Hz, 2H), 7.51 (d, $J = 7.2$ Hz, 2H), 7.47 (d, $J = 7.8$ Hz, 2H), 7.37 (d, $J = 7.8$ Hz, 2H), 7.35 (b, 2H), 6.58 (s, 2H, 23-NH), 5.32 (s, 2H, 22-NH), 4.57 (s, 2H, 24-NH), 2.78 (s, 6H, 5Me(Tol)), 2.72 (s, 6H, 20Me(Tol)), 2.62 (s, 6H, 10Me(Tol)), 2.53 (s, 6H, 15Me(Tol)), 1.41 (b, dissolved water), 0.82 (s, 2H, 21). ^{1}H NMR (600 MHz, $CDCl_3$, 213 K): δ_H 12.78 (b, 2H, 2-NH), 8.51 (d, $^3J = 7.4$ Hz, 2H, 5o'), 8.33 (d, $^3J = 7.4$ Hz, 2H, 5o), 8.12 (d, $^3J = 7.8$ Hz, 2H, 10o), 8.10 (d, $^3J = 7.4$ Hz, 2H, 5m'), 8.01 (d, $^3J = 7.4$ Hz, 2H, 5m), 7.95

(d, ^3J = 7.8 Hz, 2H, 15o), 7.94 (d, ^3J = 7.8 Hz, 2H, 20m'), 7.85 (b, 2H, 10o'), 7.84 (d, ^3J = 4.6 Hz, 2H, 7), 7.83 (b, 2H, 20o), 7.80 (d, ^3J = 4.6 Hz, 2H, 18), 7.77 (d, ^3J = 4.6 Hz, 2H, 8), 7.70 (d, ^3J = 4.8 Hz, 2H, 12), 7.68 (d, ^3J = 4.8 Hz, 2H, 13), 7.59 (d, ^3J = 7.5 Hz, 2H, 10m'), 7.592 (d, ^3J = 4.6 Hz, 2H, 17), 7.49 (d, ^3J = 7.5 Hz, 2H, 10m), 7.45 (d, ^3J = 7.8 Hz, 2H, 15m), 7.44 (d, ^3J = 7.8 Hz, 2H, 15o'), 7.39 (d, ^3J = 7.2 Hz, 4H, 20m + 20o') 7.32 (d, ^3J = 7.8 Hz, 2H, 15m'), 6.24 (s, 2H, 23-NH), 5.09 (s, 2H, 22-NH), 4.26 (s, 2H, 24-NH), 2.82 (s, 6H, 5Me(Tol)), 2.77 (s, 6H, 20Me(Tol)), 2.61 (s, 6H, 10Me(Tol)), 2.50 (s, 6H, 15Me(Tol)), 1.27 (b, 4H, associated H$_2$O), 0.58 (s, 2H, 21). ^{13}C NMR (150 MHz, CDCl$_3$, 300 K): δ_C 139.6, 139.5, 138.4, 136.9, 136.5, 136.35, 136.3, 136.2, 135.9, 135.7, 135.0, 134.3, 134.0, 132.3, 131.7, 131.4, 130.7, 129.1, 128.8, 128.7, 128.6, 127.1, 126.8, 124.8, 118.5, 116.5, 95.2 (21-C), 22.1, 21.8, 21.5, 21.4. UV−vis−near-IR (CHCl$_3$, 298 K): λ/nm (ε/M^{-1}·cm^{-1}) 282 (63 000), 342 (66 100), 397 (sh), 426 (142 400), 457 (138 800), 592 (118 800), 649 (sh), 695 (sh), 1022 (23 000). Anal. Calcd (found) for C$_{97}$H$_{83}$Cl$_7$N$_8$O$_2$: C, 71.00 (71.09); H, 5.10 (5.40); N, 6.83 (6.56).

Selected Data for **2**(HBr)$_4$(H$_2$O)$_2$. ^{1}H NMR (600 MHz, CDCl$_3$, 300 K): δ_H 12.34 (b, 2H, 2-NH), 8.43 (d, ^3J = 7.3 Hz, 4H, 5o), 8.03 (d, ^3J = 7.3 Hz, 4H, 5m), 7.95 (b, 2H, 2), 7.92 (d, ^3J = 7.3 Hz, 2H), 7.89 (d, ^3J = 4.6 Hz, 2H, 7), 7.75 (d, ^3J = 4.6 Hz, 2H), 7.70 (b, 2H), 7.66 (d, ^3J = 4.8 Hz, 2H, 12), 7.65 (d, ^3J = 4.8 Hz, 2H, 13), 7.58 (b, 2H), 7.57 (b, 2H), 7.55 (b, 2H), 7.52 (d, ^3J = 7.3 Hz, 2H), 7.46 (d, ^3J = 7.3 Hz, 2H), 7.36 (d, ^3J = 7.3 Hz, 2H), 5.84 (s, 2H, 23-NH), 5.02 (s, 2H, 22-NH), 4.35 (s, 2H, 24-NH), 2.82 (s, 6H, 5Me(Tol)), 2.76 (s, 6H, 20Me(Tol)), 2.62 (s, 6H, 10Me(Tol)), 2.52 (s, 6H, 15Me(Tol)), 0.84 (s, 2H, 21). ^{1}H NMR (600 MHz, CDCl$_3$, 213 K): δ_H 12.91 (b, 2H, 2-NH), 8.52 (d, ^3J = 7.6 Hz, 2H, 5o'), 8.33 (d, ^3J = 7.6 Hz, 2H, 5o), 8.12 (d, ^3J = 7.6 Hz, 2H, 5m'), 8.09 (b, 2H, 10o), 8.02 (d, ^3J = 7.6 Hz, 2H, 5m), 7.96 (d, ^3J = 7.8 Hz, 2H, 20m), 7.92 (d, ^3J = 7.8 Hz, 2H, 15o), 7.86 (d, ^3J = 7.7 Hz, 2H, 20o), 7.84 (d, ^3J = 4.6 Hz, 2H, 7), 7.83 (d, ^3J = 7.8 Hz, 2H, 10o'), 7.77 (d, ^3J = 4.6 Hz, 2H, 18), 7.75 (d, ^3J = 4.6 Hz, 2H, 8), 7.71 (d, ^3J = 4.8 Hz, 2H, 12), 7.69 (d, ^3J = 4.8 Hz, 2H, 13), 7.59 (d, ^3J = 7.4 Hz, 2H, 10m'), 7.56 (d, ^3J = 4.6 Hz, 2H, 17), 7.49 (d, ^3J = 7.7 Hz, 2H, 10m), 7.45 (d, ^3J = 7.8 Hz, 2H, 15m), 7.41 (d, ^3J = 7.8 Hz, 2H, 15o'), 7.39 (d, ^3J = 7.7 Hz, 2H, 20m), 7.36 (d, ^3J = 7.8 Hz, 2H, 20o'), 7.32 (d, ^3J = 7.8 Hz, 2H, 15m'), 5.60 (s, 2H, 23-NH), 4.80 (s, 2H, 22-NH), 4.03 (s, 2H, 24-NH), 2.82 (s, 6H, 5Me(Tol)), 2.77 (s, 6H, 20Me(Tol)), 2.60 (s, 6H, 10Me(Tol)), 2.50 (s, 6H, 15Me(Tol)), 1.31 (b, 4H, associated H$_2$O), 0.58 (s, 2H, 21). UV−vis−near-IR (CHCl$_3$, 298 K): λ/nm (ε/M^{-1}·cm^{-1}) 289 (sh), 349 (73 200), 429 (143 400), 458 (142 400), 596 (115 000), 658 (sh), 701 (sh), 1025 (22 100). Anal. Calcd (found) for C$_{104}$H$_{98}$Br$_4$Cl$_6$N$_8$O$_2$: C, 61.71 (62.09); H, 4.88 (5.10); N, 5.54 (5.26).

Selected Data for **2**(CH$_3$SO$_3$H)$_6$(H$_2$O)$_2$. ^{1}H NMR (500 MHz, CDCl$_3$, 300 K): δ_H 10.77 (b, 2H, 2-NH), 8.41 (d, ^3J = 7.6 Hz, 4H, 5o), 8.08 (dd, ^3J = 7.8 Hz, ^4J = 1.4 Hz, 2H, 7), 8.04 (d, ^3J = 7.6 Hz, 4H, 5m), 7.99 (b, 2H), 7.92 (d, ^3J = 4.8 Hz, 2H, 18), 7.86 (b, 2H), 7.83 (dd, ^3J = 4.8 Hz, ^4J = 1.3 Hz, 2H, 8), 7.77 (b, 2H), 7.74 (d, ^3J = 4.4 Hz, 2H, 12), 7.73 (d, ^3J = 4.4 Hz, 2H, 13), 7.69 (d, ^3J = 4.8 Hz, 2H, 17), 7.67 (d, ^3J = 7.0 Hz, 4H), 7.64 (b, 2H), 7.58 (d, ^3J = 7.6 Hz, 4H), 7.48 (b, 2H), 7.42 (b, 2H), 4.47 (b, 2H, 23-NH), 4.05 (b, 2H, 22-NH), 3.39 (dissolved water), 3.24 (b, 2H, 24-NH), 2.82 (s, 6H, 5-Me(Tol)), 2.74 (s, 6H, 20-Me(Tol)), 2.63 (s, 6H, 10-Me(Tol)), 2.52 (s, 6H, 15-Me(Tol)), 1.54 (s, 12H, CH_3SO$_3$$^-$), −0.30 (s, 2H, 21). ^{13}C NMR (126 MHz, CDCl$_3$, 300 K): δ_C 154.0, 151.7, 149.9, 149.0, 145.2, 144.0, 142.9, 142.6, 142.4, 140.0, 137.2, 136.2, 136.0, 135.8, 135.5, 134.4, 133.6, 132.1, 132.0, 130.9, 129.4, 129.1, 127.8, 122.7, 118.6, 116.8, 90.2 (21-C), 37.9 (CH_3SO$_3$$^-$), 22.1, 21.9, 21.5, 21.4. UV−vis−near-IR (CHCl$_3$, 298 K): λ/nm (ε/M^{-1}·cm^{-1}) 345 (83 000), 385 (sh), 431 (sh), 454 (192 800), 588 (110 300), 643 (sh), 692 (sh), 972 (26 900). Anal. Calcd (found) for C$_{104}$H$_{104}$Cl$_6$N$_8$O$_{20}$S$_6$: C, 57.01 (57.39); H, 4.78 (4.99); N, 5.11 (4.76); S, 8.78 (9.05).

Crystallographic Data. X-ray-quality crystals of **2** were obtained by the slow diffusion of a chloroform solution of **2** into methanol at room temperature. Crystal data for **2**: C$_{96}$H$_{74}$N$_8$·3.59CHCl$_3$·CH$_3$OH, M_r = 1798.59, T = 100(2) K, Mo Kα radiation, triclinic, space group $P\bar{1}$, a = 13.600(3) Å, b = 17.361(4) Å, c = 20.361(5) Å, α = 91.38(3)°, β = 98.78(3)°, γ = 108.92(3)°, V = 4481(2) Å^3, Z = 2, D_c = 1.333 Mg/m^3, λ = 0.710 73 Å, μ = 0.39 mm^{-1}, Oxford Diffraction Xcalibur PX diffractometer with an Onyx CCD detector, 4.7 ≤ θ ≤ 27.0°, 52 714 collected reflections, 18 894 independent reflections, 1193 parameters, R1(F) = 0.057, wR2(F^2) = 0.166, S = 0.91, largest difference peak and hole 1.24 and −0.65 e/Å^3. The structure was solved by direct methods using the *SHELXS* program.[61] All non-hydrogen atoms except for those of the disordered solvent were refined anisotropically by full matrix least squares with *SHELXL-97*.[61] All hydrogen atoms were placed in calculated positions and refined as riding models with U_{iso}(H) = 1.2U_{eq}(C).

X-ray-quality crystals of **2**(HCl)$_2$ were obtained by the slow diffusion of a chloroform solution of **2** acidified with dry HCl into hexane. Crystal data for **2**(HCl)$_2$: C$_{96}$H$_{76}$N$_8$Cl$_2$·5CHCl$_3$, M_r = 2009.39, T = 100(2) K, Cu Kα radiation, monoclinic, space group $C2/c$, a = 20.632(3) Å, b = 19.729(3) Å, c = 23.833(3) Å, β = 101.088(11)°, V = 9520(2) Å^3, Z = 4, D_c = 1.402 Mg/m^3, λ = 1.541 78 Å, μ = 0.51 mm^{-1}, Oxford Diffraction Xcalibur PX diffractometer with an Onyx CCD detector, 3.4 ≤ θ ≤ 62.9°, 8908 collected reflections, 5282 independent reflections, 584 parameters, R1(F) = 0.0838, wR2(F^2) = 0.2042, S = 0.911, largest difference peak and hole 0.56 and −0.66 e/Å^3. The structure was solved by direct methods using the *SHELXS* program.[61] All non-hydrogen atoms except for those of the disordered solvent were refined anisotropically by full matrix least squares with *SHELXL-97*.[61] All hydrogen atoms were placed in calculated positions and refined as riding models with U_{iso}(H) = 1.2U_{eq}(C).

X-ray-quality crystals of **2**(HCl)$_4$(H$_2$O)$_2$ were obtained by the slow diffusion of a chloroform solution of **2**(HCl)$_4$(H$_2$O)$_2$ into hexane. Crystal data for **2**(HCl)$_4$(H$_2$O)$_2$: C$_{96}$H$_{78}$N$_8$Cl$_4$·9.2CHCl$_3$·2H$_2$O, M_r = 2619.68, T = 100(2) K, Mo Kα radiation, monoclinic, space group $C2/c$, a = 17.170(6) Å, b = 17.695(6) Å, c = 40.55(3) Å, β = 94.06(3)°, V = 12 289(11) Å^3, Z = 4, D_c = 1.402 Mg/m^3, λ = 0.710 73 Å, μ = 0.75 mm^{-1}, KUMA KM4 CCD κ-geometry diffractometer with a Sapphire CCD detector, 3.2 ≤ θ ≤ 25.0°, 30 262 collected reflections, 10 712 independent reflections, 837 parameters, R1(F) = 0.099, wR2-(F^2) = 0.216, S = 1.14, largest difference peak and hole 0.62 and −0.59 e/Å^3. The structure was solved by direct methods using the *SHELXS* program.[61] All non-hydrogen atoms except for those of the disordered solvent were refined anisotropically by full matrix least squares with *SHELXL-97*.[61] All hydrogen atoms were placed in calculated positions and refined as riding models with U_{iso}(H) = 1.2U_{eq}(C).

Calculations. DFT calculations were performed with the *Gaussian03* program.[62] Geometry optimizations were carried out within unconstrained C_1 symmetry, with starting coordinates derived from MM+ models (*HyperChem v.7*). Becke's three-parameter exchange functionals[63] with the gradient-corrected correlation formula of Lee, Yang, and Parr (DFT−B3LYP)[64] were used with the 6-31G** basis set for all atoms. ^{1}H NMR chemical shift values were calculated by the GIAO method[65] at the same level of theory. TDDFT calculations were carried out for the lowest-energy conformers on the same level of the functional, with basis sets for 45, 55, and 60 transitions in the cases of **c**(n), **c**(d)$^{2+}$, and **tb**(q)$^{4+}$, respectively. The electronic transitions and UV−vis spectra were analyzed by means of the *GaussSum* program.[66] The transitions were convoluted by Gaussian curves with 2000 cm^{-1} half-line widths to get the calculated UV−vis−near-IR spectra.

Spectrophotometric Titrations with Acids. To a solution of **2** (3 mL, 1.27 × 10^{-5} M) in chloroform were added by a microsyringe aliquots of a TFAH or DCAH solution in CHCl$_3$ under controlled temperature conditions with constant stirring. The electronic spectra were recorded in the region of 250−1100 nm, 1 min after each addition. The arrays consisting of absorbance × wavelengths × acid concentration data were initially analyzed in order to find absorption bands that

were representative for each of the forms observed. The selected absorbance changes were analyzed by assuming equilibria of three or two consecutive forms, i.e., $(n) + (m)^+ + (d)^{2+}$ or $(d)^{2+} + (q)^{4+}$, respectively, in two carefully chosen nonoverlapping concentration ranges. Each concentration range consisted of at least 15 data points. The equilibrium concentration of the acid in each data point was estimated by means of the expressions $[HA] = c_{HA} - c_0(\Delta A^1 / \Delta A^1_\infty)$ for the first equilibrium, $[HA] = c_{HA} - c_0(1 + \Delta A^2 / \Delta A^2_\infty)$ for the second equilibrium, and $[HA] = c_{HA} - 2c_0(1 + \Delta A^4 / \Delta A^4_\infty)$ for the third equilibrium where c_{HA} is the total analytical acid concentration, c_0 is the total concentration of **2**, and $\Delta A^i / \Delta A^i_\infty$ is the ratio of the absorbance change at a given concentration of acid to the maximum change of absorbance at the wavelength chosen for each equilibrium. The absorbance data A at the representative wavelengths were fitted by means of a nonlinear curve-fitting procedure to eq 1 or 2 for the lower (0—2 equiv) or higher (2.5—30 equiv) concentration ranges, respectively:

$$A = \frac{A_n}{1 + K_1[HA] + K_1 K_2[HA]^2} + \frac{A_m}{\dfrac{1}{K_1[HA]} + 1 + K_2[HA]}$$
$$+ \frac{A_d}{\dfrac{1}{K_1 K_2[HA]^2} + \dfrac{1}{K_2[HA]} + 1} \tag{1}$$

$$A = \frac{A_d}{1 + K_4[HA]^2} + \frac{A_q}{\dfrac{1}{K_4[HA]^2} + 1} \tag{2}$$

where K_1, K_2, and K_4 are equilibrium constants for the equilibria between (n) and $(m)^+$, $(m)^+$ and $(d)^{2+}$, and $(d)^{2+}$ and $(q)^{4+}$, respectively; A_n, A_m, and A_q are the absorbances of solutions consisting solely of neutral or mono- or tetracationic form, respectively, at the concentration c_0.

Spectrophotometric Titrations with Anions. To a solution containing **2**$(BF_4)_4$ (3 mL, 1.25×10^{-5} M) in chloroform or to a solution of **2** acidified with 10 equiv of TFAH were added by a microsyringe aliquots of tetraalkylammonium salt solutions in CHCl$_3$ at 25 °C with constant stirring. The electronic spectra were recorded in the region of 250—1100 nm 1 min after each addition. The absorbance changes were fitted by assuming consecutive equilibrium of three forms: **2**$(HBF_4)_4$, **2**$(HBF_4)_2(HX)_2$, and **2**$(HX)_4$ or **2**$(TFAH)_4$, **2**$(TFAH)_2(HX)_2$, and **2**$(HX)_4$. The equilibrium concentration of the anion in each data point was estimated by means of the expression $[X^-] = c_{X^-} - 2c_0(\Delta A / \Delta A_\infty)$, where c_{X^-} is the total analytical concentration of the salt, c_0 is the total concentration of **2**, and $\Delta A / \Delta A_\infty$ is the ratio of the absorbance change at a given concentration of anion to the maximum change of absorbance at the chosen wavelength. The absorbance data A at the representative wavelengths were fitted by means of a nonlinear curve-fitting procedure to eq 3:

$$A = \frac{A_0}{1 + K_{2e}[X^-]^2} + \frac{A_2}{\dfrac{1}{K_{2e}[X^-]^2} + 1 + K_{4e}[X^-]^2} + \frac{A_4}{\dfrac{1}{K_{4e}[X^-]^2} + 1} \tag{3}$$

where K_{2e} and K_{4e} are equilibrium constants for exchange of the first or second pair of anions, respectively, and A_0, A_2, and A_4 are absorbances of solutions containing solely complex with none, two, and four anions exchanged, respectively at the concentration c_0.

■ ASSOCIATED CONTENT

ⓢ Supporting Information. Crystallographic data of **2**, **2**-$(HCl)_2$, and **2**$(HCl)_4(H_2O)_2$ in CIF format, further NMR data, DFT-calculated structures, and TDDFT-calculated electronic transitions. This material is available free of charge via the Internet at http://pubs.acs.org.

■ AUTHOR INFORMATION

Corresponding Author
*E-mail: pjc@wchuwr.pl. Fax: (+48) 71-328-2348.

■ DEDICATION

[†]Dedicated to Professor Lechosław Latos-Grażyński on the occasion of his 60th birthday.

■ REFERENCES

(1) Wiskur, S. L.; Ait-Haddou, H.; Lavigne, J. J.; Anslyn, E. V. *Acc. Chem. Res.* **2001**, *34*, 963.
(2) *Fundamentals and Applications of Anion Separations*; Singh, R. P., Moyer, B. A., Eds.; Kluwer Academic/Plenum Publishers: New York, 2004.
(3) *Anion Sensing*; Stibor, I., Ed.; Springer: Berlin, 2005.
(4) Sessler, J. L.; Gale, P. A.; Cho, W.-S. *Anion Receptor Chemistry*; Royal Society of Chemistry: Cambridge, U.K., 2006.
(5) *Structure and Bonding, Recognition of Anions*; Vilar, R., Ed.; Springer: Berlin, 2008.
(6) Best, M. D.; Tobey, S. L.; Anslyn, E. V. *Coord. Chem. Rev.* **2003**, *240*, 3.
(7) Beer, P. D.; Gale, P. A. *Angew. Chem., Int. Ed.* **2001**, *40*, 486.
(8) Beer, P. D.; Hayes, E. J. *Coord. Chem. Rev.* **2003**, *240*, 167.
(9) Choi, K.; Hamilton, A. D. *Coord. Chem. Rev.* **2003**, *240*, 101.
(10) Llinares, J. M.; Powell, D.; Bowman-James, K. *Coord. Chem. Rev.* **2003**, *240*, 57.
(11) Davis, A. P.; Joos, J.-B. *Coord. Chem. Rev.* **2003**, *240*, 143.
(12) Gale, P. A. *Coord. Chem. Rev.* **2003**, *240*, 191.
(13) Wedge, T. J.; Hawthorne, M. F. *Coord. Chem. Rev.* **2003**, *240*, 111.
(14) Hosseini, M. W. *Coord. Chem. Rev.* **2003**, *240*, 157.
(15) Bondy, C. R.; Loeb, S. J. *Coord. Chem. Rev.* **2003**, *240*, 77.
(16) Sessler, J. L.; Camiolo, S.; Gale, P. A. *Coord. Chem. Rev.* **2003**, *240*, 17.
(17) Lambert., T. N.; Smith, T. N. *Coord. Chem. Rev.* **2003**, *240*, 129.
(18) Martinez-Manez, R.; Sancenon, F. *Chem. Rev.* **2003**, *103*, 4419.
(19) Tabata, M.; Nishimoto, J. Equilibrium Data of Porphyrins and Metalloporphyrins. In *The Porphyrin Handbook*; Kadish, K. M., Smith, K. M., Guilard, R., Eds.; Academic Press: San Diego, CA, 2000; p 221.
(20) Král, V.; Andrievsky, A.; Sessler, J. L. *J. Am. Chem. Soc.* **1995**, *117*, 2953.
(21) Sessler, J. L.; Davis, J. M. *Acc. Chem. Res.* **2001**, *34*, 989.
(22) Seidel, D.; Lynch, V.; Sessler, J. L. *Angew. Chem., Int. Ed.* **2002**, *41*, 1422.
(23) Chmielewski, P. J.; Latos-Grażyński, L.; Rachlewicz, K. *Chem. —Eur. J.* **1995**, *1*, 68.
(24) Rachlewicz, K.; Sprutta, N.; Latos-Grażyński, L.; Chmielewski, P. J.; Szterenberg, L. *J. Chem. Soc., Perkin Trans. 2* **1998**, 959.
(25) Cheng, B.; Munro, O. Q.; Marques, H. M.; Scheidt, W. R. *J. Am. Chem. Soc.* **1997**, *119*, 10732.
(26) Stone, A.; Fleischer, E. B. *J. Am. Chem. Soc.* **1968**, *90*, 2735.
(27) Tsai, C.-H. T. J. Y.; Chen, J.-H.; Liao, F.-L.; Wang, S.-L.; Wang, S.-S.; Hwang, L.-P.; Chen, C.-B. *Polyhedron* **2000**, *19*, 633.
(28) Barkigia, K. M.; Fajer, J.; Berber, M. D.; Smith, K. M. *Acta Crystallogr.* **1995**, *C51*, 511.
(29) Larsen, F. B.; Hansen, F. G.; McKenzie, C. J. *Acta Crystallogr.* **2004**, *E60*, o497.

6735

dx.doi.org/10.1021/ic200742d |*Inorg. Chem.* 2011, 50, 6719–6736

(30) Finikova, O. S.; Cherpakov, A. V.; Carroll, P. J.; Vinogradov, S. A. *Inorg. Chem.* **2002**, *41*, 6944.

(31) Furuta, H.; Asano, T.; Ogawa, T. *J. Am. Chem. Soc.* **1994**, *116*, 767.

(32) De Luca, G.; Romeo, A.; Scolaro, L. M.; Ricciardi, G.; Rosa, A. *Inorg. Chem.* **2007**, *46*, 5979.

(33) Chmielewski, P. J.; Latos-Grażyński, L.; Rachlewicz, K.; Głowiak, T. *Angew. Chem., Int. Ed. Engl.* **1994**, *33*, 779.

(34) Chmielewski, P. J.; Maciołek, J.; Szterenberg, L. *Eur. J. Org. Chem.* **2009**, 3930.

(35) Furuta, H.; Ishizuka, T.; Osuka, A.; Dejima, H.; Nakagawa, H.; Ishikawa, Y. *J. Am. Chem. Soc.* **2001**, *123*, 6207.

(36) Maeda, H.; Morimoto, T.; Osuka, A.; Furuta, H. *Chem.—Asian J.* **2006**, *1*, 832.

(37) Furuta, H.; Nanami, H.; Morimoto, T.; Ogawa, T.; Kral, V.; Sessler, J. L.; Lynch, V. *Chem.—Asian J.* **2008**, *3*, 592.

(38) Osuka, A.; Shimidzu, H. *Angew. Chem., Int. Ed. Engl.* **1997**, *36*, 135.

(39) Yoshida, N.; Shimidzu, H.; Osuka, A. *Chem. Lett.* **1998**, 55.

(40) Nakano, A.; Osuka, A.; Yamazaki, I.; Yamazaki, T.; Nishimura, Y. *Angew. Chem., Int. Ed.* **1998**, *37*, 3023.

(41) Nakano, A.; Shimidzu, H.; Osuka, A. *Tetrahedron Lett.* **1998**, *39*, 9489.

(42) Ogawa, T.; Nishimoto, Y.; Yoshida, N.; Ono, N.; Osuka, A. *Chem. Commun.* **1998**, 337.

(43) Ogawa, T.; Nishimoto, Y.; Yoshida, N.; Ono, N.; Osuka, A. *Angew. Chem., Int. Ed.* **1999**, *38*, 176.

(44) Yoshida, N.; Osuka, A. *Tetrahedron Lett.* **2000**, *41*, 9287.

(45) Tsuda, A.; Nakano, A.; Furuta, H.; Yamochi, H.; Osuka, A. *Angew. Chem., Int. Ed.* **2000**, *39*, 558.

(46) Wojaczyński, J.; Latos-Grażyński, L.; Chmielewski, P. J.; Van Calcar, P.; Balch, A. L. *Inorg. Chem.* **1999**, *38*, 3040.

(47) Deng, Y.; Chang, C. K.; Nocera, D. G. *Angew. Chem., Int. Ed.* **2000**, *39*, 1066.

(48) Bringmann, G.; Rüdenauer, S.; Götz, D. G. C.; Gulder, T. A. M.; Reichert, M. *Org. Lett.* **2006**, *8*, 4743.

(49) Bringmann, G.; Goetz, D. C. G.; Gulder, T. A. M.; Gehrke, T. H.; Bruhn, T.; Kupfer, T.; Radacki, K.; Braunschweig, H.; Heckmann, A.; Lambert, C. *J. Am. Chem. Soc.* **2008**, *130*, 17812.

(50) Chmielewski, P. J. *Angew. Chem., Int. Ed.* **2004**, *43*, 5655.

(51) Siczek, M.; Chmielewski, P. J. *Angew. Chem., Int. Ed.* **2007**, *46*, 7432.

(52) Chmielewski, P. J. *Angew. Chem., Int. Ed.* **2005**, *44*, 6417.

(53) Chmielewski, P. J.; Durlej, B.; Siczek, M.; Szterenberg, L. *Angew. Chem., Int. Ed.* **2009**, *48*, 8736.

(54) Dippy, J. F. J.; Hughes, S. R. C.; Rozanski, A. *J. Chem. Soc.* **1959**, 2492.

(55) Lide, D. R. *Handbook of Chemistry and Physics*; CRC Press: Boca Raton, FL, 1998; p 1278.

(56) Stępień, M.; Szyszko, B.; Latos-Grażyński, L. *J. Am. Chem. Soc.* **2010**, *132*, 3140.

(57) Perepichka, D. F.; Bryce, M. R. *Angew. Chem., Int. Ed.* **2005**, *44*, 5370.

(58) Kurotobi, K.; Kim, K. S.; Noh, S. B.; Kim, D.; Osuka, A. *Angew. Chem., Int. Ed.* **2006**, *45*, 3944.

(59) Davis, N. K. S.; Thompson, A. L.; Anderson, H. L. *J. Am. Chem. Soc.* **2011**, *133*, 30.

(60) Geier, G. R., III; Haynes, D. M.; Lindsey, J. S. *Org. Lett.* **1999**, *1*, 1455.

(61) Sheldrick, G. M. *Acta Crystallogr.* **2008**, *A64*, 112.

(62) Frisch, M. J.; Trucks, G. W.; Schlegel, H. B.; Scuseria, G. E.; Robb, M. A.; Cheeseman, J. R.; Montgomery, J. A.; Vreven, T.; Kudin, K. N.; Burant, J. C.; Millam, J. M.; Iyengar, S. S.; Tomasi, J.; Barone, V.; Mennucci, B.; Cossi, M.; Scalmani, G.; Rega, N.; Petersson, G. A.; Nakatsuji, H.; Hada, M.; Ehara, M.; Toyota, K.; Fukuda, R.; Hasegawa, J.; Ishida, M.; Nakajima, T.; Honda, Y.; Kitao, O.; Nakai, H.; Klene, M.; Li, X.; Knox, J. E.; Hratchian, H. P.; Cross, J. B.; Adamo, C.; Jarmillo, J.; Gomperts, R.; Stratmann, R. E.; Yazyev, O.; Austin, A. J.; Cammi, R.; Pomelli, C.; Ochterski, J.; Ayala, P. Y.; Morokuma, K.; Voth, G. A.; Salvador, P.; Dannenberg, J. J.; Zakrzewski, V. G.; Dapprich, S.; Daniels, A. D.; Strain, M. C.; Farkas, O.; Malick, D. K.; Rabuck, A. D.; Raghavachari, K.; Foresman, J. B.; Ortiz, J. V.; Cui, Q.; Baboul, A. G.; Clifford, S.; Cioslowski, J.; Stefanov, B. B.; Liu, G.; Liashenko, A.; Piskorz, P.; Komaromi, I.; Martin, R. L.; Fox, D. J.; Keith, T.; Al-Laham, M. A.; Peng, C. Y.; Nanayakkara, A.; Challacombe, M.; Gill, P. M. W.; Johnson, B. G.; Chen, W.; Wong, M. W.; Gonzales, C.; Pople, J. A. *Gaussian03*, revision C.01; Gaussian, Inc.: Pittsburgh, PA, 2004.

(63) Becke, A. D. *J. Chem. Phys.* **1993**, *98*, 5648.

(64) Lee, C.; Yang, W.; Parr, R. G. *Phys. Rev. B* **1988**, *37*, 785.

(65) Wolinski, K.; Hinton, J. F.; Pulay, P. *J. Am. Chem. Soc.* **1990**, *112*, 8251.

(66) O'Boyle, N. M.; Tenderholt, A. L.; Langner, K. M. *J. Comput. Chem.* **2008**, *29*, 839.